(Proposal to Jefferson Lab PAC 39)

Measurement of the Ratio $R = \sigma_L/\sigma_T$ in Exclusive and Semi-Inclusive π° Production

May 4, 2012

A. Camsonne, S. Covrig, P. Degtiarenko, R. Ent (co-spokesperson), D. Gaskell, M.K. Jones, V. Kubarovksy, P. Nadel-Turoński, B. Sawatzky, P. Solvignon, M. Ungaro, S.A. Wood

Jefferson Lab, Newport News, VA 23606

I. Albayrak, M. Carmignotto, J. Dénes-Couto, N. Hlavin, T. Horn (co-spokesperson)[1], F. Klein, M. Metz, B. Nepal, L. Rothgeb

The Catholic University of America, Washington, DC 20064

O. Ates, M.E. Christy, C. Jackson, C.E. Keppel, N. Kalantarians, M. Kohl, P. Monaghan, A. Pushpakumari, L. Tang, J. Taylor, T. Walton

Hampton University, Hampton, VA 23668

A. Asaturyan, A. Mkrtchyan, H. Mkrtchyan (co-spokesperson), V. Tadevosyan, S. Zhamkochyan

A.I. Alikhanyan National Science Laboratory, Yerevan 0036, Armenia

C. Hyde

Old Dominion University, Norfolk, Virginia

M. Guidal, C. Munoz Camacho

Institut de Physique Nucleaire d'Orsay, IN2P3, BP 1, 91406 Orsay, France

A. Gasparian

North Carolina A&T University, Greensboro, NC 27411

M. Khandaker, V. Punjabi

Norfolk State University, Norfolk, VA 23504

F. Sabatié

CEA-Saclay, Service Physique Nucléaire, F91191 Gif-sur-Yvette, France

G.M. Huber, W. Li

University of Regina, Regina, Saskatchewan, Canada, S4S 0A2

E. Brash

Christopher Newport University, Newport News, Virginia

D. Dutta

Mississippi State University, Mississippi State, MS

G. Niculesu, I. Niculescu

James Madison University, Harrisonburg, Virginia

Y. Illieva, S. Strauch

University of South Carolina, Columbia, South Carolina

P. Markowitz. J. Reinhold

Florida International University, Miami, Florida

A. Sarty

Saint Mary's University, Halifax, Canada

P. King, J. Roche

Ohio University, Athens, OH 45701

J. Arrington, K. Hafidi, P. Reimer

Argonne National Laboratory, Argonne, IL

P. Stoler

Rensselaer Polytechnic Institute, Troy, NY 12180-3590

I. Bedlinskiy

ITEP, Moscow, Russia

[1] Contact person: hornt@jlab.org

Abstract

The neutral pion electroproduction reaction is an important tool in our study of hadron structure. The quantum numbers in the π° production process introduce sensitivity to axial vector configurations. The pion-exchange contributions in the t-channel are expected to be suppressed. Despite these positive aspects, this reaction has been relatively unexploited to date because of the lack of the necessary experimental facilities. As a result, there are practically no L/T separated data for semi-inclusive (elasticity $z < 1$) or exclusive ($z \to 1$) π° production from the proton.

With the unique capabilities of the 12 GeV upgrade, we have the opportunity to dramatically improve upon this situation and measure observables, in particular the ratio $R = \sigma_L/\sigma_T$ for neutral-pion electroproduction, hitherto only known as model-dependent guesses. This proposal has the following primary goals:

- The L/T separated cross sections in the exclusive limit $z \to 1$
  Separated p$(e, e'\pi^\circ)$p cross sections allow investigations of the transition from hadronic to partonic degrees of freedom in exclusive processes. Recent separated π^+ data from JLab suggest that the power-law behavior expected from the hard-scattering mechanism is reasonably consistent with the dependence on Q^2, the four-momentum transfer squared, of longitudinal cross section data. However, the transverse cross section does not show a corresponding behavior, indicating that transversely polarized photons may play an important role in pion electroproduction even at relatively high values of Q^2. The Q^2-dependence of the pion form factor is likewise consistent with the Q^2-scaling expectation already at values of $Q^2 > 1$ GeV^2, while the observed magnitude is larger than the hard QCD prediction. Charged pion processes feature a meson exchange contribution in the t-channel (pole term), whose impact on factorization has to be understood. Hence, it is of great interest to study a similar system in which the pole term is suppressed. A direct comparison of the π° longitudinal and transverse cross sections and their ratio for Q^2 up to 5.1 GeV^2 would thus be essential for our understanding of the transition from the hadronic to the partonic regime. We thus propose a systematic measurement of the Q^2-dependence of the L/T separated cross sections at fixed x_B=0.5 in neutral pion electroproduction. In the hard scattering regime, one may expect that the longitudinal and transverse cross section scale as Q^{-6} and Q^{-8}, respectively. A large value of their ratio R would be indicative of the realization of the scaling expectation of the factorization theorem for helicity non-flip GPDs, while a large transverse cross section could suggest contributions from transversity (helicity flip) GPDs.

  The coupling to a virtual photon is suppressed for the neutral pion, and so the pion exchange contribution in the t-channel (pion pole) to the longitudinal cross section is suppressed as well. This is different from the charged pion case, where the pion pole is dominant. Our proposed measurement of the t and x dependence of the π° longitudinal cross section, using L/T separated p$(e, e'\pi^\circ)$p cross section data, will thus also allow to constrain the size of the non-pole contributions in charged-pion electroproduction. One study predicts that the perturbative QCD longitudinal cross section is comparable in size for both the π^+ and π° [1]. This is different from the simpler interpretation that $\sigma_L \approx 0$ for neutral-pion electroproduction, since the pion exchange diagram does not contribute. Thus, a significant longitudinal response in forward π° electroproduction may be indicative of non-pole contributions in forward charged-pion electroproduction.

- The L/T separated cross sections in the regime $z < 1$
  Whereas inclusive scattering cannot distinguish between the quark flavor, there is great promise in flavor decompositions of regular or transverse-momentum dependent parton distributions through semi-inclusive deep inelastic scattering, and of generalized parton distributions through deep exclusive scattering. For the latter, the ratio $R = \sigma_L/\sigma_T$ asymptotically scales like Q^2 at fixed Bjorken x. For the former, the ratio R is usually assumed by analyzers of semi-inclusive deep inelastic scattering (SIDIS) data to be either zero or equal to the values determined from inclusive deep inelastic scattering.

Measurements of the behavior of R in SIDIS have direct relevance for the planned polarized SIDIS experiments at JLab at 12 GeV that focus on transverse momentum dependent parton distributions (TMDs) and corresponding angular asymmetries. Fractional uncertainties in the latter are roughly equal to $\epsilon\delta R$. For $\epsilon \approx 0.5$ they are roughly 50% of the uncertainty in R, which as indicated above can be quite large, and z and Q^2 dependent. Measurements of R in SIDIS will also help to shed light on the nature of the SIDIS process, particularly important at the modest energies of JLab where target and hadron mass corrections may become relevant (especially in the $z \to 1$ limit), and deviations of the Leading-Order factorized picture likely contribute, and provide valuable information about the size of higher-twist contributions at JLab energies. For instance, the TMD formalism predicts that $\sigma_L = 0$ at subleading order $\sim 1/Q$.

The ratio R for semi-inclusive neutral-pion electroproduction may at low energies very well depend on z, Q^2, and p_T, the transverse pion momentum. Furthermore, data from this proposed experiment and the anticipated precision L/T data for SIDIS with charged-meson production (E12-06-104), may make comparisons of π^+, π^- and π° possible, which would allow for a precision verification of the often-assumed yet naive relation $\pi^\circ = (\pi^+ + \pi^-)/2$. In the kaon case, for example, there seems a huge difference between $D_u^{K^+}$ and $D_{\bar{s}}^{K^+}$, which naively would be the same given that $K^+ = u\bar{s}$. Though one may be led to believe that $D_{\bar{s}} > D_u$ since the u and s masses are much different, the opposite seems to be true [2]. Furthermore, in the limit $z \to 1$ one would definitely anticipate the behavior of R for π° to differ from that for $(\pi^+ + \pi^-)/2$, given that the exclusive limit has no pole contributions. At the modest energies of JLab-12 GeV this has implications for the higher-twist contributions. The proposed measurements are thus both of fundamental and of practical value.

We thus propose to perform measurements of the L/T separated cross sections and their ratio $R = \sigma_L/\sigma_T$ in neutral-pion electroproduction over a range in z from 0.4 to 1.0, *i.e.*, covering both the deep exclusive and semi-inclusive deep inelastic scattering regions. Note that at the recommendation of PAC38 we have placed the emphasis in the choice of kinematics on the deep-exclusive data, but with the proposed setup exclusive and semi-inclusive data are accumulated simultaneously. This approach also addresses the renewed theoretical interest in the connection between these processes, with the Giessen group calculating the transverse cross sections in the exclusive limit by a DIS-like Lund hadronization Ansatz.

The measurement can be adequately performed using the existing and well-understood Hall C High-Momentum Spectrometer to detect the scattered electrons. The neutral pion will be detected by measurement of its $\gamma\gamma$ decay products in a dedicated neutral-pion detector. We plan to use a conventional sweeping magnet, similar but with only ∼10% of the field requirements as the Horizontal-Bend magnet presently under construction for the new Hall C/SHMS to maintain access to low-angle π° detection, and the high-resolution lead-tungsten $PbWO_4$ crystals of the PRIMEX experiment to construct a 25 msr neutral-pion detector at a distance of 4 meter from the target (1116 crystals). The setup will be remotely rotatable in the $\sim 6^\circ$-30° angle region using cantelevered platforms of the SHMS spectrometer.

Detailed background simulations show this setup allows for 1 μA beam current on a 10 cm long cryogenic LH2 target. We will simultaneously map the L/T separated deep-exclusive $p(e,e'\pi^\circ)p$ and semi-inclusive $p(e,e'\pi^\circ)X$ cross sections and their ratios at energies of 6.6, 8.2, 8.8, 10.8 and 11 GeV, requesting 62 PAC days. We have in addition included two kinematics (five PAC days) to increase the ϵ lever arm for semi-inclusive measurements and one series of measurements (two days) on a 10 cm long cryogenic LD2 target solely driven by the semi-inclusive $d(e,e'\pi^\circ)X$ reaction to constrain the behavior of R for deuterons, in analogy with the approved $d(e,e'\pi^\pm)X$ reactions. The total beam time request thus corresponds to 69 PAC days.

Contents

I. CONTRIBUTION TO THE HALL C 12 GEV UPGRADE

The co-spokespersons for this experiment plan to contribute to the implementation of the Hall C upgrade for 12 GeV in both manpower and materials.

The Catholic University of America group with Tanja Horn as one of the spokespersons for this proposal leads a consortium (Catholic University of America, University of South Carolina, Mississippi State University, and Florida International University) that was awarded a Major Research Instrumentation grant from the National Science Foundation for construction of a kaon identification system, consisting of a pair of aerogel detectors, for the Hall C SHMS. This consortium acquired photomultiplier tubes and aerogel material from the MIT/BLAST experiment to augment this effort. The construction of the mechanical frames for the detector and their assembly are nearing completion in the CUA workshop.

The Catholic University of America group, leading a consortium of Old Dominion University and Florida International University, also submitted a Major Research Instrumentation grant in support of developing the general-purpose Hall C π° detection system described in this proposal. In particular, the neutral-pion detector system utilizes a dedicated sweeping magnet (a low-field version of the Horizontal Bend magnet for the SHMS presently under construction), and the $PbWO_4$ crystals of the PRIMEX apparatus, with a new dedicated temperature-controlled frame, cantelevered stands, and new digitizing electronics. The CUA group intends to provide the manpower in support of the R&D, construction, and commissioning of this detector system.

The Yerevan group with Hamlet Mkrtchyan as one of the spokespersons of this proposal has taken on responsibility of assembling and testing the calorimeter for the SHMS. The blocks and PMTs for this calorimeter are a contribution to the 12-GeV Upgrade project by Yerevan and NIKHEF. The Yerevan group has also worked on the research and design related to the choice of calorimeter blocks, and confirmation of the suitability of the contributed calorimeter blocks (previously used in the HERMES experiment), as well as the engineering and design. The preshower detector will consist of calorimeter blocks presently in the SOS spectrometer. The Yerevan group is committed to further construction and subsequent commissioning of the complete SHMS electromagnetic calorimeter. Given their lead role in the design and construction of the HMS aerogel detector, the Yerevan group also collaborates on the testing and construction of the SHMS kaon identification system mentioned above. The contribution of the Yerevan group, to the calorimeter and other projects is up to 3 full-time equivalents (FTEs).

The Hampton group (M.E. Christy, R. Ent, C.E. Keppel, P. Monaghan et al.) is part of a consortium (with the College of William and Mary (lead), James Madison University and North Carolina A&T), that have obtained an NSF/MRI grant to construct the SHMS tracking and trigger detectors (consisting of the wire chambers, scintillators, quartz detector, and their detector frame). Hampton's commitment in this consortium is to the (design and) construction and commissioning of the SHMS wire chambers. Hampton also plans to provide personnel for new HMS wire chambers, of similar design as the new SHMS wire chambers. This will replace the aged present HMS chambers.

II. SCIENTIFIC MOTIVATION

The electromagnetic interaction has proven very successful in probing the structure of the nucleon in a quest to understand the strong interactions between quarks, and the gluons that bind them. In general, electron scattering experiments can be classified into inclusive, exclusive, and semi-inclusive categories. In an inclusive electron scattering experiment, only the scattered electron is detected. In exclusive electron scattering, both the scattered electron and all final state particles are detected (or reconstructed by kinematics). In semi-inclusive scattering, one of the final-state hadrons is measured in coincidence with the scattered electron.

Considerable information on nucleon structure has been extracted over the past few decades from separations of inclusive lepton-nucleon cross sections, at high four-momentum transfer squared, Q^2, and high excitation energy, ν (corresponding to large missing mass W), into longitudinal and transverse structure functions. For example, early measurements of the structure function F_2 were shown to exhibit a (logarithmic) scaling behavior at fixed Bjorken $x = Q^2/2M\nu$, and were subsequently shown to be related to the momentum distribution of the quarks inside the nucleon in terms of parton distribution functions, whose universal nature makes them useful in understanding a wide variety of particle interactions with nucleons.

The original experimental observation (at large Q^2) of the smallness of the ratio $R = \sigma_L/\sigma_T$, the ratio of the contributions to the measured cross section from longitudinally and transversely polarized virtual photon scattering, respectively, as measured in deep inelastic scattering (DIS), provided the first evidence of the fundamental spin-1/2 nature of the partons. At lower Q^2, the ratio becomes sensitive to indirect gluon effects and higher-twist contributions, and is in the naive quark-parton model related to the parton's average transverse momentum $\langle k_t^2 \rangle$: $R = 4(M^2x^2 - \langle k_t^2 \rangle)/(Q^2 + 2\langle k_t^2 \rangle)$.

Since that time, separated structure functions F_2 and R have been measured in DIS over a wide range of Q^2 and x, at CERN, SLAC, and DESY. More recently, the first precision separated measurements of the proton and deuteron structure functions R and F_2 were performed at JLab, mainly emphasizing the nucleon resonance region but also extending into the DIS region. The value of the inclusion of such L/T separated structure function data is apparent from recent work [3]. Relatively good constraints on the large-x gluon can be obtained from the scaling violations of F_2, provided that a weak cut on invariant mass W is considered and higher twist terms are included, as shown in the CJ fits [4]. Inclusion of F_L data in global fits is expected to provide direct constraints on gluons. The recent JLab data for F_L at low $Q^2 < 4$ GeV^2, in particular, allow to considerably extend the reach in x. These data already allowed the first determination of F_L moments from world data over a large Q^2 range, and suggest either the presence of significant higher twist effects in F_L or a large gluon distribution at high x [3].

It has been long realized that more stringent tests of the quark-parton model arise from more exclusive hadron production experiments. In particular, processes whose common feature is the tagging of the active parton provide unique tools for probing the flavor, tranverse momentum, and spatial structure of the nucleon. The most general case of those is the semi-inclusive deep inelastic scattering process in which one produces any number of final-state particles and tags the one that contains the active parton. If one restricts the reaction so that no additional final-state particles are produced (elasticity $z \to 1$) one can probe the transverse spatial structure of the nucleon through Generalized Parton Distributions. An important aspect of accessing the transverse spatial structure is that one must demonstrate that factorization of hard and soft physics applies. Factorization has been proven for longitudinal photons in [5]. On the experimental side, as noted in the PAC38 report [6], the π° separated longitudinal and transverse cross sections and their ratio in the exclusive $z \to 1$ limit are essentially unknown. These are important quantities since factorization has only been proven for the longitudinal component of the cross section, which is related unambigously with Generalized Parton Distributions (GPDs). As remarked in an earlier PAC32 report [7] it is important to experimentally determine the longitudinal cross section (or put a boundary on its value) for the proper interpretation of the results. Furthermore, there has been a renewed theoretical interest in the relative role of longitudinally and transversely polarized photons in the context of

transversity GPDs as discussed in, e.g., [8, 9]. These new theoretical developments strengthen the case for L/T separated exclusive π° cross sections to provide a reliable interpretation of results from the 12 GeV JLab GPD program.

Here, we will concentrate on one of the simplest cases, neutral-pion electroproduction. This channel is of particular interest as it will shed light on our understanding of a partonic description of pion electroproduction in both the semi-inclusive and (deep) exclusive case. The lack of pole contributions make the study of the neutral-pion channel particularly attractive.

Specifically, the ratio R is assumed by analyzers of semi-inclusive deep inelastic scattering data to be either zero or equal to the values determined from inclusive deep inelastic scattering. This is independent of the particular meson probed. On the other hand, in the exclusive $z \to 1$ limit, there is a fundamental difference between charged-pion and neutral-pion electroproduction in that the latter process has no pole contributions. Yet, in the perturbative limit non-pole contributions may easily provide a substantial longitudinal cross section, similar for both charged-pion and neutral-pion electroproduction, and asymptotically make $R \sim Q^2$ for both processes. Thus, it is of great interest to compare the inclusive-exclusive connection of neutral-pion and charged-pion electroproduction.

Comparison between exclusive charged and neutral pion production will further quantify the impact of non-trivial non-pole contributions in pion electroproduction, which would be a great leap forward in our understanding of meson electroproduction. If these non-pole backgrounds are smaller than anticipated this may also dramatically increase the kinematic range accessible for measurements of the charged pion form factor at 12 GeV.

A. The π° L/T separated cross sections for $z < 1$

Experience with inclusive Deep Inelastic Scattering clearly shows that L/T separated cross sections provide much more insight into parton model dynamics and its limits than the unseparated ones. We once more point to the value of the inclusion of L/T separated structure function data in global fits, as exhibited in recent work [3].

Measurements of the behavior of $R = \sigma_L/\sigma_T$ in Semi-Inclusive Deep Inelastic Scattering (SIDIS) are expected to particularly shed light on the underlying partonic nature of the SIDIS process. Verifying whether $R_{SIDIS} = R_{DIS}$ in deep-inelastic kinematics is a test of the dominance of the electron-quark scattering followed by a quark fragmentation process. As compared to deep-inelastic scattering, the inclusive hadron production process may allow for flavor decomposition of the contributions of transverse momentum widths to R. This correlation has recently been more rigorously worked out as part of the transverse momentum dependent (TMD) parton distribution formalism. There are indications of an x, energy, and flavor dependence of the widths of these functions.

Further understanding of the underlying parton dynamics of the SIDIS process is particularly important at the modest energies of JLab where deviations of the Leading-Order factorized picture likely contribute. In agreement with the asymptotic $1/Q^2$ dependence of R, the TMD formalism predicts that the longitudinal cross section vanishes at leading order, $\sim 1/Q$, or at twist-3 level. The size of σ_L/σ_T measured for neutral-pion electroproduction can thus provide valuable information about the size of twist-4 contributions at JLab energies. The $z \to 1$ limit is also of interest from the perspective of hadron mass corrections, both in terms of finite values of target mass M^2/Q^2 and produce hadron mass m_π^2/Q^2 relative to the virtual photon mass Q^2 (~ 4 GeV^2) [11]. As such, there is direct relevance for the planned polarized SIDIS experiments at JLab at 12 GeV that focus on transverse momentum dependent parton distributions and corresponding angular asymmetries. Fractional uncertainties in the latter are roughly equal to $\epsilon\delta R$, so for $\epsilon \approx 0.5$ roughly 50% of the uncertainty in R, which is at the moment unconstrained, and anticipated to be Q^2 and z dependent.

In SIDIS there exist extra kinematical degrees of freedom associated with the detected hadron. With the positive z-axis in the direction of the electromagnetic current, two further variables can be chosen to characterize the problem: the hadron transverse momentum p_T and the elasticity z. As a result, there will be in general four structure functions for the $(e, e'\pi)$ coincidence process, the usual longitudinal and transverse structure functions and two additional interference structure functions. Measurements of the $\cos(\phi)$ and $\cos(2\phi)$ dependencies to constrain these interference structure functions are now thought to shed light on the transverse motion of quarks, assuming parton dynamics. Within this proposal, we will mostly concentrate on a p_T region where we have access to the full ϕ acceptance, such that in principle we can remove sensitivity to these interference structure functions in SIDIS kinematics by integration.

The ratio R for semi-inclusive neutral-pion electroproduction may at low energies depend on z, Q^2, and p_T, the transverse pion momentum. In fact, a pronounced dependence on the z of the measured hadron is expected, where its exact behavior is of fundamental interest for understanding the parton dynamics underlying hadron production. Unlike the case of the L/T separations for charged pion SIDIS, the topic of the approved E12-06-104 experiment, the $z \to 1$ limit for neutral-pion electroproduction is anticipated to differ at modest Q^2. At asymptotic energy values, the L/T ratio for both deep exclusive charged- and neutral pion electroproduction is expected to scale like Q^2. For modest energies, the exclusive neutral-pion electroproduction process does not have pole contributions, unlike the charged-pion case, and one anticipates a drastically different L/T behavior.

Having data in hand for this proposed experiment, and the anticipated precision L/T data for SIDIS with charged-meson production of E12-06-104, one may make comparisons between π^+, π^- and π°, which would allow for a precision verification of the often-assumed relation $\pi^\circ = (\pi^+ + \pi^-)/2$. One would anticipate that in the limit $z \to 1$ the behavior of R for π° must differ from this often-used yet naive assumption. In the kaon case, for example, there seems a huge difference between $D_u^{K^+}$ and $D_{\bar{s}}^{K^+}$, which naively would be the same given that $K^+ = u\bar{s}$. Of course the masses of u and s are much different, which may lead one to believe that $D_{\bar{s}} > D_u$, but the opposite seems true. Furthermore, in the limit $z \to 1$ one would definitely anticipate the behavior of R for π° to differ from that for $(\pi^+ + \pi^-)/2$, given that the exclusive limit has no pole contributions. Thus, comparisons of π° and $\pi^\pm$ L/T ratios will provide valuable information on the size of non-leading twist contributions at JLab energies and potential further parton dynamics and model extractions. For instance, they would directly allow to revisit the inclusive-exclusive connection dating back to the 1970s in a new fashion, for instance extending the realizations within the constituent quark model of duality in several symmetry breaking scenarios from charged-pion to neutral-pion electroproduction [10]. As indicated above, semi-inclusive data in the limit of $z \to 1$ would also constrain target and hadron mass corrections [11]. Thus, the proposed measurements are both of fundamental and of practical value for the SIDIS studies at JLab and beyond.

B. The π° L/T separated cross sections in the limit $z \to 1$

The importance of π° L/T separated cross sections goes back to the factorization of hard and soft physics needed for the interpretation of GPD results.

The QCD-parton picture of the hadron predicts a separation of short-distance and long-distance physics at sufficiently high Q^2. Measurements of inclusive processes, such as deep-inelastic scattering (DIS), confirm that in the limit of large Q^2, at fixed values of x, such processes can be viewed as scattering from individual partons within the hadronic system. A similar separation (factorization) of scales may be expected to apply to hard exclusive scattering and allow the use of perturbative QCD (pQCD) concepts for exploring hadron structure.

One prediction of the factorization theorem is that in the limit of large Q^2, the dominant virtual photon polarization is longitudinal. The corresponding cross section scales to leading order like $\sigma_L \sim Q^{-6}$ at fixed x and $-t$, modulo higher order corrections [5, 12]. The contribution of transversely polarized photons is suppressed by an additional power of $1/Q$ in the amplitude. In the Q^2-scaling limit, pQCD describes the short distance process

and Generalized Parton Distributions (GPDs) provide access to the non-perturbative physics.

Recent π^+ data from JLab indicate a $1/Q^6$-scaling of the longitudinal cross section (σ_L) that is consistent with a hard scattering mechanism already at values of $Q^2 > 1$ GeV^2 [13], but the transverse cross section (σ_T) does not show a corresponding $1/Q^8$ behavior. This may suggest that transversely polarized photons play an important role in pion electroproduction. This is supported by recent experimental results from the HERMES collaboration [14] showing a large $\sin\phi_s$ modulation of the π^+ electroproduction cross section that does not seem to vanish in the forward direction which, model-independently, implies a large amplitude for a helicity +1 photon and proton helicity flip [15]. Preliminary CLAS data [16] on π^0 electroproduction provide another hint at contributions from γ_T^*: the absolute value of the transverse-transverse interference cross section amounts to a substantial fraction of the unseparated cross section (except for small scattering angles). As has been pointed out in [8, 15] this requires contributions from the transversity (helicity flip) GPDs, in particular from H_T and $\bar{E}_T = 2\widetilde{H}_T + E_T$ [17, 18] along with twist-3 pion wave functions. The amplitudes for transversely polarized photons are parametrically suppressed by μ_π/Q as compared to the asymptotically leading amplitudes for longitudinally polarized photons (related to the usual GPDs $\widetilde{H}$ and $\widetilde{E}$). The parameter μ_π is fixed by the divergency of the axial-vector current and amounts to 2 GeV (at a scale of 2 GeV). This would suggest that there is no strong suppression of the transverse amplitudes at values of Q^2 accessible in present-day experiments. It would thus be of great interest to determine the relative longitudinal and transverse contributions to the π° cross section.

At high Q^2, pion electroproduction probes the polarized quark GPDs $\tilde{E}$ and $\tilde{H}$. In the limit $t \to m_\pi^2$, the π^+ production amplitude contains a "pole term" governed by the pion form factor, which in the region $x_B > 0.1$ is governed at high Q^2 by the hard scattering mechanism. The pion pole appears as a strong singularity in the function $\tilde{E}^u - \tilde{E}^d$, and is generally assumed to dominate over the regular part of the amplitude. Although it is known that the pion pole contribution is suppressed in π° production because the direct coupling with a virtual photon is suppressed, our understanding of the reaction mechanism in π° electroproduction is far from clear. This is further exemplified by the recent successful description of the transverse cross sections of the exclusive π^+ electroproduction process by the Giessen group, where such transverse cross sections are counterintuitively well described with a DIS-like Lund model hadronization approach, in which the $\gamma^* q \to q$ scattering process is followed by the fragmentation of an excited colored string, using the PYTHIA/JETSET implementation [19].

Another formalism for describing the transverse cross section has recently been presented in [8]. In this formalism, the amplitudes for transversely polarized photons are parametrically suppressed as compared to the asymptotically leading amplitudes for longitudinally polarized photons related to the usual GPDs. This would suggest that transverse amplitudes may be large at low values of Q^2 allowing access to the helicity flip GPDs. These new theoretical developments strengthen the case for L/T separated exclusive π° cross sections to provide a reliable interpretation of results from the 12 GeV JLab GPD program.

By comparing the π^+ and π° longitudinal and transverse production amplitudes, one can further quantify the impact of the non-pole contributions in pion electroproduction. Measurements of the Q^2 dependence for L/T separated cross sections in the Q^2=1-5 GeV^2 region, accessed by this proposal, would thus be a great leap forward in our understanding of meson electroproduction even if the onset of asymptotic scaling only occurs at very high values of Q^2.

III. ELECTROPRODUCTION OF π° AND RELATED PROCESSES – PREVIOUS DATA AND ANALYSES

A. Inclusive Scattering

For inclusive electron-nucleon scattering the differential cross section can, in the one-photon approximation, be written as:

$$\frac{d^2\sigma}{d\Omega_e dE'} = \sigma_{Mott}\{W_2(Q^2,W^2) + 2W_1(Q^2,W^2)tan^2(\theta/2)\}, \tag{1}$$

with σ_{Mott} the Mott cross section defined as

$$\sigma_{Mott} = \frac{\alpha^2\cos^2(\theta/2)}{4E^2 sin^4(\theta/2)} \tag{2}$$

and W_1 and W_2 the structure functions that contain information about the electromagnetic structure of the nucleon.

In the Bjorken limit, in which both Q^2 and $\nu \to \infty$, but x is fixed, the structure functions W_1 and W_2 were found to exhibit scaling. Therefore, it was convenient to introduce the dimensionless functions F_1 and F_2, defined by

$$F_1(x,Q^2) \;=\; MW_1(\nu,Q^2)\;, \tag{3}$$

$$F_2(x,Q^2) \;=\; \nu W_2(\nu,Q^2)\;. \tag{4}$$

In the quark-parton model these F_1 and F_2 structure functions are given in terms of parton distributions, $q(x)$ and $\bar{q}(x)$,

$$F_2(x) = 2xF_1(x) = x\sum_q e_q^2\left(q(x) + \bar{q}(x)\right)\;, \tag{5}$$

where $q(x)$ is interpreted as the probability to find a quark of flavor q in the nucleon with light-cone momentum fraction x. Here, one can directly see that inclusive scattering can only probe the sum of, but not the individual, parton distributions.

The inclusive cross section can also be expressed in terms of σ_T and σ_L, the cross sections for the absorption of transverse and longitudinal photons, respectively. From this perspective, the ratio of longitudinal to transverse cross sections is expressed as

$$R \equiv \frac{\sigma_L}{\sigma_T} = \frac{F_2}{2xF_1}\left(1 + \frac{4M^2x^2}{Q^2}\right) - 1\;. \tag{6}$$

Note that while the F_1 structure function is related only to the transverse virtual photon coupling, F_2 is a combination of both transverse and longitudinal couplings. For historical reasons, the world DIS data is expressed in terms of F_2 and R. For asymptotic energies, $R \to 1/Q^2 \to 0$, a consequence of the scattering of (asymptotically free) spin-1/2 constituents. At lower and finite Q^2, the ratio becomes sensitive to indirect gluon effects and higher-twist contributions, and is in the naive quark-parton model related to the parton's average transverse momentum $\langle k_t^2\rangle$: $R = 4(M^2x^2 - \langle k_t^2\rangle)/(Q^2 + 2\langle k_t^2\rangle)$.

Within the phase space available at 12-GeV JLab, R remains rather constant to only drop $\sim 1/Q^2$ beyond $Q^2 \sim 3$ GeV^2 [20]. All DIS measurements of R on deuterium (for $Q^2 > 1$ GeV^2) are found to be in excellent agreement with the data on hydrogen, so to very good approximation $R^p = R^d$ for DIS. The relevance to include F_L separated structure function data to global fits was recently discussed, with considerable extension in the range of x, for gluon knowledge and higher-twist constraints.

B. Semi-Inclusive Scattering

In the one-photon exchange approximation, the pion electroproduction cross section can in general be written as the product of a virtual photon flux (Γ) and a virtual photon cross section (evaluated in the laboratory frame),

$$\frac{d\sigma}{d\Omega_e dE_e d\Omega_\pi dM_x} = \Gamma\frac{d\sigma}{d\Omega_\pi dM_x}\;, \tag{7}$$

where M_x is the missing mass of the recoiling system, $M_x^2 = (q + P_A - p_\pi)^2$. The virtual photon flux is given by

$$\Gamma = \frac{\alpha}{2\pi^2}\frac{E'_e}{E_e}\frac{1}{Q^2}\frac{1}{1-\epsilon}\frac{W^2 - M^2}{2M} \ . \tag{8}$$

Here, ϵ is the virtual-photon polarization. The virtual-photon cross section can be written as

$$\frac{d\sigma}{d\Omega_\pi dM_x} \ = \ \frac{d\sigma_T}{d\Omega_\pi dM_x} + \epsilon\frac{d\sigma_L}{d\Omega_\pi dM_x} + \epsilon\frac{d\sigma_{TT}}{d\Omega_\pi dM_x}\cos 2\phi_{pq} + \sqrt{2\epsilon(1+\epsilon)}\frac{d\sigma_{LT}}{d\Omega_\pi dM_x}\cos\phi_{pq} \ , \tag{9}$$

where ϵ describes the longitudinal polarization of the virtual photon. In parallel kinematics, the interference terms (σ_{LT} and σ_{TT}) are small, and for complete ϕ ($= \phi_{pq}$) coverage integrate to zero. The cross sections can be parameterized in terms of four structure functions, W_L, W_T, W_{TT} and W_{LT}, that in general now depend on Q^2, W^2, z and p_T. For the case of exclusive ($z = 1$) electroproduction cross sections, the formalism is identical, but the four structure functions are in general expressed as dependent on Q^2, W^2 and the Mandelstam variable t reflecting the four-momentum transfer to the final state. The differential cross section is then often described in terms of $dtd\phi$ rather than $d\Omega_\pi$.

In the Bjorken limit, these formulas should simplify again, and can be more intuitively expressed in a quark-parton model. From perturbative QCD, there now will be factorization between the virtual photon–quark interaction and the subsequent quark hadronization,

$$\frac{dN}{dz} \sim \sum_q e_q^2 \ q(x,Q^2) \ D_{q\to\pi}(z,Q^2), \tag{10}$$

where the fragmentation function $D_{q\to\pi}(z,Q^2)$ gives the probability for a quark to evolve into a pion π detected with a fraction z of the quark (or virtual photon) energy, $z = E_\pi/\nu$. Within such an asymptotic description, it is natural to assume the ratio R for SIDIS to equate the ratio R found for the DIS electron-quark scattering process, and this has often been assumed by analyzers of SIDIS data. However, in the general formalism there may very well be dependence of R on the additional degrees of freedom z and p_T, and in fact this is expected from a hadronic description at low-intermediate Q^2. In the $z \to 1$ limit the $R_{SIDIS} = R_{DIS}$ assumption even **must** fail, as R must become dependent on z.

In the asymptotic limit, in the model where the electro-produced pions are the fragmentation products of spin-1/2 partons, the ratio $R = \sigma_L/\sigma_T$ must vanish like $1/Q^2$, like in the inclusive case. This idea is supported by the measurement of angular distributions of hadrons in the process $e^+e^- \to h + X$, with h a hadron, for spin-1/2 partons. At high energies, the JADE experiment [21] at a center-of-mass energy of 35 GeV, and the OPAL and DELPHI experiments at the Z-pole [22, 23] show a longitudinal to total cross section ratio well consistent with either JETSET [24] or a second-order QCD calculation [25]. At a lower center-of-mass energy of 7.4 GeV, this ratio, and hence R, is found to depend on z, approaching small numbers for $z \to 1$, where the observed hadrons (pions) are thought to only be emitted by spin-1/2 partons.

In SIDIS, the only available data are from Cornell, where in the early 1970s a series of measurements of semi-inclusive pion electroproduction was carried out at Cornell with both hydrogen and deuterium targets [26–28]. This series of measurements covered a region $1 < Q^2 < 4$ GeV^2 and $0.1 < z < 0.9$. However, the lack of precision of the Cornell data makes the ratio R be consistent with both what would be expected from R in DIS and with a null value. As a function of z, some hint of an increase of R at larger $z \sim 0.8$ may exist, at a 2σ level. The Cornell experiments also included a series of L/T measurements for the semi-inclusive (e,e′p) reaction, measuring a fast proton. The data were not sufficient to make quantitative statements on the L/T character, and agreed with zero within large uncertainties. This is the only data set to some extent related to the present proposed L/T separations in the neutral-pion channel. In general, there are no L/T separated data at all for the (e,e′π°) reaction in the deep inelastic region.

More recently, E00-108 [29] measured the ^{1,2}H(e,e′$\pi^\pm$)X unseparated cross sections, predominantly at x = 0.32. The data conclusively showed the onset of the quark-hadron duality phenomenon in the semi-inclusive

(e,e′π) process, and the relation of this to the high-energy factorization ansatz of subsequent electron-quark scattering and quark → pion production. Agreement between data and Monte Carlo simulation, based upon CTEQ5M parton distributions [30] and BKK fragmentation functions [31], was found to be excellent for $z < 0.65$ (or $M_x^2 > 2.5$ GeV^2: note that within the E00-108 kinematics $p_T \sim 0$, and M_x^2 is almost directly related to z, as $W'^2 \equiv M_x^2 = M_p^2 + Q^2(1/x - 1)(1 - z)$). Simple ratios constructed from the data following quark-parton model descriptions were found to be remarkably close to the near-independence of z as anticipated in the high-energy limit (at leading order in α_S). These findings have led to a rich and industrious SIDIS program at JLab at both 6 GeV, and soon 12 GeV.

E00-108 did not accumulate L/T separated data and always assumed $R_{SIDIS} = R_{DIS}$. Of course, if integrated over z, p_T, ϕ, and all hadrons, this must be true. The semi-inclusive (e,e′h) structure functions in general depend on additional variables beyond x and Q^2, in particular on z and p_T, and the ratio R_{SIDIS} could very well depend on z, and should so at low-intermediate Q^2.

In this proposal we only emphasize the low p_T region, < 0.4 GeV, where we have access to the full ϕ acceptance (see the E12-06-104 and E12-09-017 proposals [32, 33] and Figure 2(a)), and will map what the ratio R is for neutral-pion electroproduction, mainly off a proton target but with one select set of measurements off a deuteron (neutron) target. The specific dependence of R on z is anticipated to be fundamentally different for π° and $\pi^\pm$ electroproduction at low-intermediate Q^2, as the hadronic description of the exclusive limit will be different. In addition, this will imply that locally assumptions such as π° yields average charged-pion π^+ and π^- yields must fail. This naive relation fails drastically for the kaon case. Knowledge of R for the (e,e′π°) process is also required for planned polarized SIDIS experiments at JLab at 12 GeV and corresponding angular asymmetries of neutral-pion electroproduction. Due to its exceptional character (as compared to its charged family members), knowledge of R on neutral-pion electroproduction with strikingly different expectations, seems to be the key to make progress on the transition to a partonic description of semi-inclusive and deep exclusive measurements.

C. Exclusive Electroproduction of π°

Previous experimental exclusive π° electroproduction data in the limit $z \to 1$ above the resonance region are available from Hall B [34, 35] and Hall A [36, 37].

One of the goals of the Hall B measurements was to study the onset of the partonic reaction mechanism. The differential cross section for meson production was measured in a kinematic region of W=2.1-2.7 GeV covering a range in Q^2 of 1 to 5 GeV^2 and momentum transfers $-t$=0.1-5 (GeV/c)^2. Preliminary results for the η production cross section can be found in reference [38]. Though the extraction of the interference terms can be achieved using the CLAS acceptance, the measured cross sections cannot be separated into the components corresponding to longitudinally and transversely polarized photons without assumptions on each contribution. The nonzero beam spin asymmetries determined in this measurement imply that both longitudinal and transverse cross sections participate in the process. Thus, additional information on the relative size of longitudinal and transverse components is of interest for further interpretation of these existing data sets, the kinematic reach of which overlaps with the kinematics proposed for this measurement.

A clean L/T separation of the components of the cross sections may also be of interest to the study of exclusive π° cross sections with CLAS12 [38]. The main focus of that experiment is comprehensive studies of exclusive π° and η production including the detailed investigation of factorization predictions. Part of the measurement is dedicated to the study of π° separated cross sections. However, depending on the absolute size of σ_L a detailed study of the separated π° cross section using CLAS12 alone may be complicated. If σ_L is non-negligible, precision measurements of the separated cross sections require additional information from double-arm spectrometer setups like the ones in Hall A and Hall C. Thus, the separated results from the proposed

measurement may influence part of the final design of the 12 GeV π° program. Our kinematics are thus complementary to those of E12-06-108: the additional information on the relative size of longitudinal and transverse components of the cross section, important in understanding the onset of factorization, would allow for a more reliable interpretation of the CLAS12 data.

The unseparated cross sections were measured with the E00-110/DVCS setup in Hall A at x_B=0.37 between Q^2=1.94 GeV^2 and Q^2=2.35 GeV^2 giving a lever arm of ΔQ^2=0.4 GeV^2. The results suggested a potentially sizeable contribution of the longitudinal cross section. Furthermore, the unseparated cross section showed no dependence on t. This measurement was extended by E07-007, in which a separation of the cross section will be attempted at x_B=0.37 between Q^2=1.5 GeV^2 and Q^2=2.3 GeV^2 giving a lever arm of ΔQ^2=0.8 GeV^2. Our data are complementary to these two measurements and extend the lever arm to nearly ΔQ^2=2 GeV^2. This will be important in evaluating the Q^2-dependence of the separated cross section for signs of scaling trends. Our scan in t may also shed light on the lack of t dependence observed in E00-110.

The separated cross section data and the neutral pion detector can also be important for the extension of other experiments, for example, the Hall A "Deeply Virtual Compton Scattering (DVCS)" experiment. The exclusive portion of the experiment proposed here, can measure the H$(e,e'\gamma)p$ Deeply Virtual Compton Scattering (DVCS) reaction simultaneously [39]. Although the Hall A E12-06-114 DVCS experiment [40] will cover a wide kinematic range, there is a range of kinematics not accessible with high precision in Hall A, due to the limited momentum range of the Hall A High Resolution Spectrometers (HRS). The first Hall A measurements [41, 42] provided stringent constraints on the approach to QCD factorization for $Q^2 \sim 2\,\mathrm{GeV}^2$. A second experiment, completed in 2010 [43], had the goal of separating the real part of the DVCS† Bethe-Heitler interference from the DVCS-squared term by a generalized Rosenbluth technique of measurements at fixed Q^2, x_B, and t, while varying the beam energy. Extending this program of separations to 12 GeV kinematics requires the larger momentum range of the Hall C HMS spectrometer. The neutral pion experiment proposed here will provide an initial separation for DVCS. Upon completion of this project, extensions to a broader kinematic range are anticipated.

Experiments using the recoil polarization technique detecting a forward proton were performed at JLab in Hall A ([44–46]) as well as at Mainz [47]. The main goal of experiment E93-103 was the study of the quadrupole strength around the Δ resonance using recoil polarization at Q^2=1.0 GeV^2. The comprehensive angular coverage included data sensitive to the longitudinal polarization of the photon. A separation of the longitudinal π° cross section was attempted, but currently no official publication of these data is available. Most of the earlier exclusive π° electroproduction data including [48] are limited to center of mass energies in the resonance region and cannot be easily separated due to kinematic constraints. The recoil technique relies on the resolution of the reconstructed missing mass to control background contributions, but the resolution deteriorates with increasing center of mass energy. It would thus be of great interest to understand the backgrounds by first conducting an experiment with direct detection of the π°.

IV. EXPERIMENTAL METHOD

We propose to measure the L/T separated cross sections for the elementary neutral-pion electroproduction reaction using the Rosenbluth separation technique ranging in elasticity, z, from 0.4 to 1.0, the exclusive limit.

We illustrate the kinematics of the exclusive p$(e,e'\pi^\circ)$p reaction in Figure 1. The incident electron with four momentum k=(E_e,$\mathbf{k}$) scatters through an angle θ_e to a final four momentum q=(ω,$\mathbf{q}$). The electron scattering plane is defined by the three-momenta $\mathbf{k}$ and $\mathbf{k}'$, and also includes the exchanged virtual photon three momentum transfer $\mathbf{q}$. The virtual photon is absorbed by the target proton and a pion is emitted with four-momentum p'_π=($E(p'_\pi)$, p_π), where p_π is oriented relative to the scattering plane by a polar angle θ_{π° and an azimuthal angle ϕ_{π°. In this experiment we will reconstruct the proton. This means that the only restriction

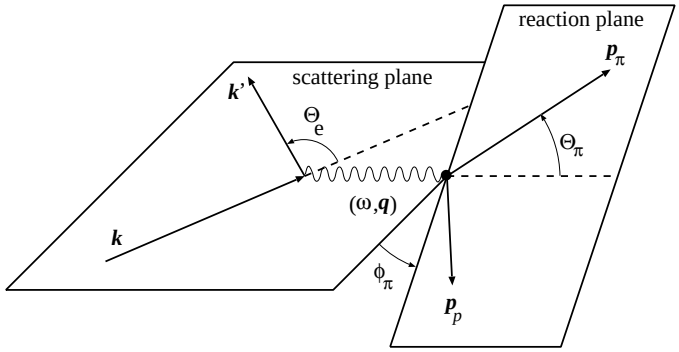

FIG. 1: *Kinematics of the $p(e,e'\pi^\circ)p$ reaction.*

on the coverage in t at any given electron angle comes from the acceptance of the π°-calorimeter. More details about the detector can be found in section IV B.

The unpolarized pion electroproduction cross section can be written as the product of a virtual photon flux factor and a virtual photon cross section,

$$\frac{d^5\sigma}{d\Omega_e dE'_e d\Omega_{\pi^\circ}} = J\left(t,\phi\rightarrow\Omega_\pi\right)\Gamma_v\frac{d^2\sigma}{dtd\phi}, \tag{11}$$

where $J\left(t,\phi\rightarrow\Omega_{\pi^\circ}\right)$ is the Jacobian of the transformation from $dtd\phi$ to $d\Omega_{\pi^\circ}$, and Γ is the virtual photon flux factor as defined in equation 8. The virtual photon cross section can be expressed in terms of contributions from transversely and longitudinally polarized photons,

$$2\pi\frac{d^2\sigma}{dtd\phi} = \frac{d\sigma_T}{dt} + \epsilon\frac{d\sigma_L}{dt} + \sqrt{2\epsilon(1+\epsilon)}\frac{d\sigma_{LT}}{dt}cos\phi + \epsilon\frac{d\sigma_{TT}}{dt}cos2\phi. \tag{12}$$

Here, $\epsilon = \left(1+2\frac{|\mathbf{q^2}|}{Q^2}\tan^2\frac{\theta_e}{2}\right)^{-1}$ is the virtual photon polarization, where $\mathbf{q^2}$ is the square of the three-momentum transferred to the nucleon. The interference terms, σ_{LT} and σ_{TT}, can be eliminated by averaging over ϕ_{π°, and the longitudinal and transverse cross sections can be separated by measuring the cross section at two or more values of ϵ.

As shown in figure 2(a) we will have full coverage over ϕ_{π° up to transverse momentum of p_T=0.4 (GeV/c)^2 and thus eliminate any dependence on the interference terms. This coverage is sufficient for the proposed L/T separations at $z < 1$.

On the other hand, for the exclusive data it is not always possible to measure the $-t$ dependence of the cross section in parallel kinematics, since W, Q^2, and $-t$ are not independent variables. In order to measure this $-t$ dependence one must vary θ_{π° away from parallel kinematics. In this case σ_{LT} and σ_{TT} also contribute and additional data are required for a complete ϕ_{π° coverage. The interference terms can then be obtained from the ϕ_{π° dependence of the data. Nevertheless, as illustrated in Figure 2(b) for Q^2=2 GeV^2 and x=0.2 the t-coverage of the experiment is uniform to about t=0.3 (GeV/c)^2 and is thus adequate to obtain the cross section in parallel kinematics.

A. Experimental overview

In this experiment we propose to make coincidence measurements between scattered electrons in the existing HMS and photons from the decay of neutral pions in a neutral-pion channel using a $PbWO_4$ calorimeter. The $PbWO_4$ calorimeter will detect photons corresponding to π° electroproduction close to the direction of $\vec{q}$ (parallel

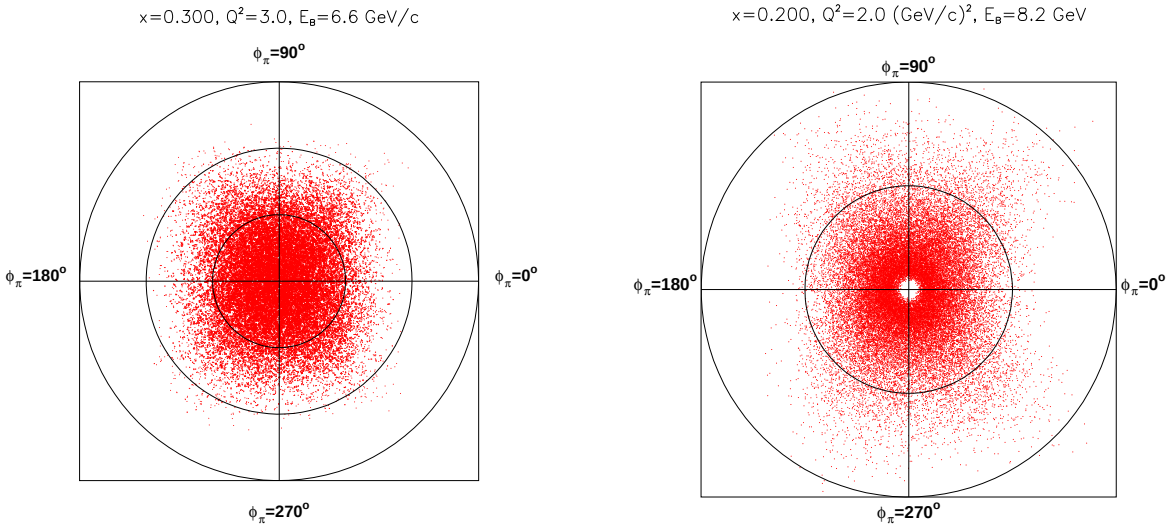

(a) *ϕ vs. p_T. The radial divisions correspond to p_T=0.2, 0.4, 0.6 (GeV/c)^2.*

(b) *ϕ vs. t. The radial divisions correspond to t=0.3, 0.6 (GeV/c)^2.*

FIG. 2: *Simulated p_T and t (radial coordinate) vs. azimuthal angle ϕ distributions for the proposed measurement.*

kinematics). These events correspond to θ_{π° near zero degrees. A high luminosity spectrometer+calorimeter system like the HMS+$PbWO_4$ combination in Hall C is well suited for such a measurement. The magnetic spectrometers benefit from relatively small point-to-point uncertainties, which are crucial for meaningful L-T separations. In particular, the optics properties and the acceptance of the HMS have been studied extensively and are well understood in the kinematic range between 0.5 and 5 GeV, as evidenced by more than 200 L/T separations ($\sim$ 1000 kinematics) [49]. The position of the elastic peak has been shown to be stable to better than 1 MeV, and the precision rail system and rigid pivot connection have provided reproducible spectrometer pointing for about a decade.

A large acceptance device like CLAS12 is well suited for measuring pseudoscalar meson electroproduction over a large range of $-t$ and x_B. Though the large azimuthal coverage allows for a good determination of the interference terms, the main constraint is the error amplification in the extraction of longitudinal and transverse components. The use of the HMS and $PbWO_4$ calorimeter in Hall C is proposed here as their characteristics best address the experimental requirements, and the existing knowledge of the properties of the HMS is expected to allow for a well understood isolation of the longitudinal cross section on the order of seventy days.

We intend to perform all measurements on a hydrogen target, apart from the necessary Al "dummy" measurements for target wall subtraction, and one series of measurements on a deuterium target to verify if $R^H_{SIDIS} = R^D_{SIDIS}$ for semi-inclusive neutral-pion electroproduction, in a kinematics region overlapping with many SIDIS experiments at JLab-12 GeV intending to do flavor decompositions.

The goal of the experiment is to accumulate coincidence $(e, e'\pi^\circ)$ data with the HMS and a dedicated, yet flexible neutral-pion detector setup. However, we will in addition accumulate HMS single-arm (e,e$'$) triggers to facilitate the semi-inclusive data analysis by forming direct ratios of semi-inclusive and inclusive yields while minimizing systematics. For the exclusive data, they will provide a direct luminosity determination. More information on the triggers will be given in sections IV D and IV G. We expect the systematic uncertainties of the proposed measurements to be only slightly larger than those for equivalent charged-pion measurements.

B. Neutral-Pion Detection System

We will construct a general-purpose and remotely rotatable neutral-pion detection system for Hall C. A floor layout of the HMS and the proposed rotatable neutral-pion detection system is shown in Fig. 3(a). This neutral-pion detection system consists of the following elements:

- A sweeping magnet providing 0.3 Tm field strength, with similar outer geometry as the Horizontal-Bend (HB) Magnet presently under construction for the SHMS but conventional copper coils.
- A neutral-pion detector consisting of 1116 $PbWO_4$ blocks of the PRIMEX experimental setup in a new temperature controlled frame, comprising a 25 msr device at a distance of 4 meters.
- Essentially deadtime-less digitizing electronics to independently sample the entire pulse form for each crystal allowing for background subtraction and identification of pile-up in each signal. This is a major improvement over the existing PRIMEX apparatus.
- A new set of high voltage distribution bases with built-in amplifiers for operation in high-rate environments.
- Cantelevered platforms of the SHMS carriage, to allow for precise and remote rotation around the Hall C pivot of the full neutral-pion detection system, over an angle range between 6 and 29 degrees.
- A dedicated beam pipe with as large critical angle as possible to reduce backgrounds beyond the HB-type sweeping magnet.

To provide space for this sweeping magnet, the HB magnet for the SHMS needs to be removed. As discussed below this is not a real issue. The HB adds a 3 degree horizontal pre-bend to the SHMS to allow reaching the smallest angles, as compared to an 18 degreee vertical bend. Thus, it only provides a small perturbation to the SHMS optics, and as such removing and reinstalling the HB magnet does not impact the final SHMS optics understanding, given proper attention to alignment. In fact, the SHMS is in this sense comparable to the earlier SOS optics, where removing and properly reinstalling and realigning the SOS quadrupole did not imply additional optics understanding work beyond the standard sieve-slit calibration runs.

The sweeping magnet will be a conventional version of the HB magnet presently under construction, with copper coils to effectively use the full bore of such a magnet (35 by 36 cm^2). In sharp contrast to the superconducting HB magnet, which provides a field strength of 1.93 Tm, we only require a 0.3 Tm field to sweep away charged particles up to 300 MeV/c. This modest field requirement is well within the range of conventional magnet coils, alleviating the need for additional cryogenic and inner vacuum cans. The sweeping magnet design is matched to existing JLab power supplies and existing commercial conductors. The materials for the coil, a 24 m of copper conductor of dimension 0.5x0.5 in^2, including a 1/4 inch diameter water cooling channel, could be obtained from, for instance, Luvata-Finnland. The coil winding tools could be obtained through AES-Penn. The materials for the yoke steel could be obtained from vendors like Oakland Steel and would be purchased in slabs of 4" for easier machining in university machine shops. These magnet component vendors also supplied the respective components for the Hall A PREX magnet. The estimated radiation dose at the location of the magnet ($<$ 30,000 rem/hr) was folded into decisions for radiation hard resins and insulation systems.

The obvious advantage of using a sweeping magnet cloning the geometric properties of the HB magnet is that it has a relatively large bore, of 35 by 36 cm^2, and is designed from the start to reach small scattering angles without impacting the main electron beam. The effective gap for an HB-type magnet for neutral particle may be slightly reduced, as the coil assumes a 3 degree horizontal pre-bend for charged particles. Thus, if we assume a direct clone of the HB the effective gap for neutral particles (assuming symmetric acceptance around the detection angle) is reduced to about 30 by 36 cm^2. This problem likely gets alleviated for a conventional magnet but we have assumed the latter aperture for the rate estimates. We found that we can move the "HB-clone" sweeping magnet about 20 cm forwards as compared to the HB, such that the magnetic center is at a

(a) (b)

FIG. 3: *(a)The π° detector in Hall C. The cylinder at the top center is the (1 m diameter) vacuum chamber containing the 10 cm long liquid-hydrogen target. The long yellow tube emanating from the scattering chamber on the lower right is the downstream beam pipe. To the left of the beam pipe is the HMS. Only the liquid He and liquid N_2 lines for the large superconducting quadrupoles at the entrance to the spectrometer are clearly visible. To the right of the beam line, the first quadrupole of the SHMS and its cryogenic feed lines are shown. This spectrometer will be used for π° experiments as a carriage to support the $PbWO_4$ calorimeter (shown in its light-tight and temperature control box next to the beam line) and the associated sweep magnet. (b) The high resolution $PbWO_4$ part of the HYCAL on which the present design is based.*

distance of 1.57 m from the pivot. This then constitutes a solid angle of 25.5 msr, with ∼146 mrad horizontal and ∼175 mrad vertical acceptance (taking into account a vacuum can of 1 meter length). Projecting this to a distance of 4 meters, the front face of the $PbWO_4$ calorimeter, implies a detector of 58 cm wide and 70 cm high. This corresponds to 29 by 34 $PbWO_4$ crystals of 2.05 by 2.05 cm^2 (each 18.0 cm long). We have added one crystal on each side to properly capture showers, and thus designed our $PbWO_4$ calorimeter to consist of 31 by 36 $PbWO_4$ crystals, or 64 by 74 cm^2. This amounts to a requirement of 1116 $PbWO_4$ crystals, less than the 1152 used in the Hybrid Calorimeter of the PRIMEX experiment.

To reject high-energy charged particles that are not deflected by the sweeper magnet, 5 mm-thick, segmented scintillator counters could be installed in front of the $PbWO_4$ crystals. The space between the HB magnet and the $PbWO_4$ detector will be enclosed within a vacuum channel (with a thin exit window, reducing remaining low-energy background) to minimize the decay photon conversion in air.

The scintillation light output of the $PbWO_4$ crystals is temperature sensitive, and thus the entire calorimeter must be kept at a constant temperature (to within 0.1° to guarantee 0.5% energy stability for absolute calibration and resolution). Furthermore, the high-voltage dividers on the PMTs may dissipate a total of several hundred Watts, and this power must not create temperature gradients or instabilities in the calorimeter. The π^0 calorimeter will thus be thermally isolated and surrounded on all four sides by water cooled copper plates. This design is based on that of the HYCAL temperature controlled frame and optimized with more recent experience from CMS [63], which has shown stability to 0.05° C. The design accomodates a geometrical arrangement in an array of 36 by 31 crystals. The materials for the frame include steel and steel alloy plates, copper plates, and a temperature control system. The setup has been shown to be compatible with the lowest π° central detection angle of 6.3 degrees required in this experiment * (see Fig. 3(a)).

* The π^0 scattering angles cover 6.3-24.0 degrees where the angles smaller than 8.6 degrees are only relevant for SIDIS.

At the anticipated background rates (see section VIII), pile-up and the associated baseline shifts can adversely affect the calorimeter resolution, thereby constituting the limiting factor for the beam current. The solution is to read out a sampled signal, and perform offline shape analysis using a flash ADC (fADC) system (see section IV D). New HV distribution bases with built-in pre-amplifiers (see section IX) will allow for operating the PMTs at lower voltage and lower anode currents, and thus protect the photocathodes or dynodes from damage.

The $PbWO_4$ π° detector is located at a distance of 4 meters, and the dimensions of the $PbWO_4$ crystals are 2.05 x 2.05 cm^2. The typical position resolution is 2-3 mm. Each crystal covers 5 mrad, and the expected angular resolution is 0.5-0.75 mrad, which is comparable with the resolutions of the HMS and SOS, routinely used for Rosenbluth separations in Hall C. This can also be compared with the CLAS Inner Calorimeter (IC), which has crystals of dimensions 1.33 x 1.33 cm^2 at the front face, located at a distance of 0.8 m from the target. The CLAS IC has reached an angular resolution of 3-4 mrad [50]. Note that as compared to the CLAS IC the solid angle per crystal reduces in our case by a factor of 2.1.

The momentum resolution for exclusively-produced neutral-pions amounts to better than 1%. All these are sufficient given the anticipated less-drastic t-dependence of exclusive ^{1}H(e,e$'\pi^\circ$)p channel as compared to ^{1}H(e,e$'\pi^+$)n.

C. Geometric acceptance of the π° detector

Neutral pion $N(e,e'\pi^\circ)X$ will generate both $N(e,e'\gamma)\gamma X$ and triple $N(e,e'\gamma\gamma)X$ events. Only events with two photons will be used to determine the π° electroproduction cross sections. The $\pi^\circ \to \gamma\gamma$ decay is isotropic in the pion rest frame. For exclusive π° production, there is a strong forward boost of the decay toward the calorimeter resulting in good π° acceptance. For neutral pions following a semi-inclusive scattering process, the acceptance will become negligible at small z where the $\gamma\gamma$ decay angle becomes large, preventing coincidence γ detection. In our experimental configuration this happens at $z \sim 0.3$, where the pion energy is reduced to $E_\pi \sim$ 1.5 GeV.

The geometric acceptance of the π° detector was estimated by means of a Monte Carlo calculation. Direction of the primary π° was sampled within the geometric acceptance of the detector, with subsequent π° decay into two γ's. The fraction of events where both γ's were simultaneously detected in the calorimeter was used to calculate the acceptance.

The pions originated from a distance of 4 meters to the calorimeter. A Gaussian distribution of transverse momentum of the π° relative to the direction of the virtual photon was assumed. The virtual photon pointed to the center of the calorimeter, and the slope parameter of the exponential transverse momentum p_T distribution, b=4.661 $(\mathrm{GeV/c})^{-2}$, was taken similar to charged pion production. The prompt pion decay in two photons was sampled uniformly in π° CM frame, and then the γ's were boosted into the lab frame. Cases with both γ's hitting the active area of the calorimeter and energies of at least 100 MeV were scored.

The geometric acceptance for the chosen configuration of the detector at different kinematic settings are listed in Table I. The acceptance rises with pion energy due to the decrease in the $\gamma\gamma$ opening angle.

As shown in Table 4, the π° energies will range from 2.1 to 5.3 GeV. Even at the highest energies, the opening angle will be of the order of 50 mrad, providing ample separation between the two shower centroids given the expected angular resolution of about 0.7 mrad of the π° detector.

To estimate the efficiency of selecting the photon pair from π° decay from other processes at forward angles, several background simulations were performed to study the combinatoric background. For the worst case scenario, and using a 100 ns coincidence time window for the two photons, the combinatoric background is already only at the few % level, as shown in Figure 4, even at the worst-case smallest angle of 6.3 degrees before application of any other cuts. Thus, we feel confident that we can understand the efficiency, and especially the stability of the absolute detector efficiency, well under the assumptions of a 1 μA beam current and a 10 cm long

z	E_{π^0} (GeV)	acceptance (%)
0.40	2.132	9.43 ± 0.03
0.50	2.665	20.23 ± 0.04
0.60	3.198	29.92 ± 0.05
0.70	3.731	38.47 ± 0.05
0.80	4.264	45.91 ± 0.05
0.90	4.797	52.42 ± 0.05
1.00	5.330	58.26 ± 0.05

TABLE I: *Geometric acceptance of π° detection in a calorimeter with an 58 × 70 cm^2 active area at 4 m distance from target. The acceptance is quoted as relative to the overall ∼25 msr opening angle. The uncertainty only presents the random sampling accuracy.*

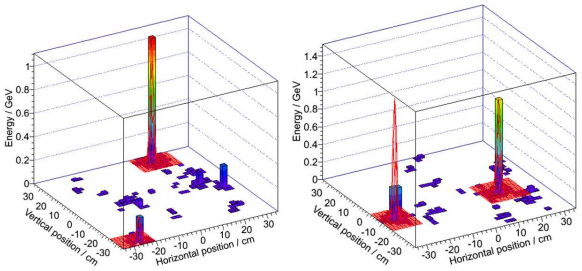

(a) *GEANT4 simulation of photons from π° decay with simulated background of neutral and charged particles, the latter suppressed by the sweeper magnet. The photon pair is selected from other processes in the calorimeter using a cluster finding algorithm.*

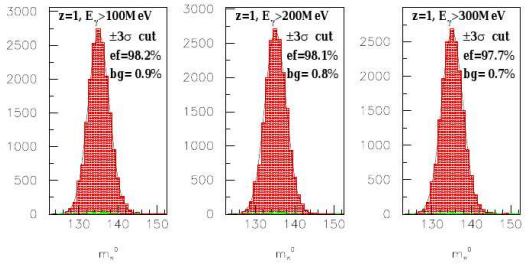

(b) *Reconstructed invariant mass of the π°.*

FIG. 4: Simulations of the $PbWO_4$ calorimeter.

LH2 target.

To elucidate this further, we present in Figure 5 the anticipated pion detection efficiency and combinatoric background as a function of electronics threshold. This is estimated based upon realistic background simulations by P. Degtiarenko for a 10 cm liquid hydrogen target at 1μA, at the worst case smallest angle of the settings (6.3° †). We also note that the 10 cm liquid hydrogen target and 1μA assumptions are very reasonable and we expect to understand the π° detection efficiency and combinatoric background well under these conditions and

† The π^0 scattering angles cover 6.3-24.0 degrees where the angles smaller than 8.6 degrees are only relevant for SIDIS.

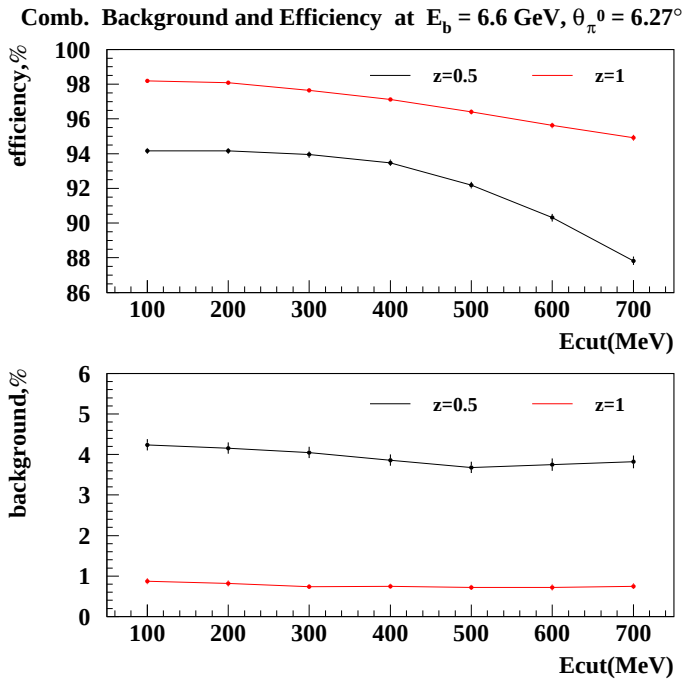

FIG. 5: The pion detection efficiency and combinatoric background as a function of threshold.

even more so in the exclusive limit.

D. Electronics for Neutral-Pion Detector

Both photons following the decay of neutral pions will be detected in the $PbWO_4$ calorimeter, with geometric acceptance as presented above. In this section we will describe the plans for the electronics and π° trigger.

Both photons following the decay of neutral pions have to be detected in coincidence with the scattered electron. However, for all of the currently anticipated kinematics, the singles rate of electrons in the HMS will be sufficiently low (<1kHz) to allow using a minimum-bias electron trigger and reading out the π° calorimeter in each event. In this way, exclusive, semi-inclusive, and inclusive cross sections can be compared directly at each kinematic point.

To take full advantage of the high-resolution crystals while operating in a high-background environment, modern flash ADCs (fADCs) will be used to digitize the signal. They continuously sample the signal every 4 ns, storing the information in an internal FPGA memory. When a trigger is received, the samples in a programmable window around the threshold crossing are read out for each crystal that fired. Since the readout of the FPGA does not interfere with the digitizations, the process is essentially deadtime free. If needed, the DAQ system will support windows up to 200-300 ns at 1 kHz and 100% occupancy in the 1200 channel calorimeter ($\sim$ 200 MB/s), but projected data rates will be smaller by orders of magnitude for all kinematics even if the thresholds are set very low. The sampled signals can then be fitted and integrated off-line, effectively eliminating issues with pile-ups, baseline shifts, etc.

For low-Q^2 measurements, where the electron singles rate could be high, the fADC-based system can also support a coincidence trigger. Such a trigger would take advantage of the ability of the fADC to perform the integration of the pulse and pass it along to the trigger for cluster finding. The appropriate conditions for the

latter can then be used to select, for instance, π° or DVCS events. The integration and cluster finding will delay the trigger decision, but this can be easily accomodated in a pipelined system without any need for delay cables or analog delay modules. In summary, the system will provide a low dead time, precision signal processing off-line, and support both high-rate operations in singles mode as well as advanced, trigger-level cluster finding in coincidence mode, As such, it will not only constitute a major advance compared with previous systems used at JLab (*e.g.*, in Hall A), but also make the most effective use of the existing hardware ($PbWO_4$ crystals).

E. Radiation condition and Luminosity Limits

To preserve a high and constant neutral-pion trigger efficiency during the experiment, special attention must be paid to the calorimeter radiation damage in order to avoid problems when using a high threshold in the trigger electronics. Radiation damage is determined by both instantaneous dose rate and integrated dose. The radiation dose absorbed by the calorimeter blocks at angles less than 10° is dominated by Moeller electrons.

For the $PbWO_4$ crystals such radiation effects have been tested in HEPI (Protvino, Russia), at Brookhaven National Laboratory, and at CERN. At low dose rates (15-20 krad/h or less), and at integrated doses below 10 krad only 2-3% degradation effects of the $PbWO_4$ have been observed [51]. The radiation damage dramatically increases at higher doses. For example, at a dose rate of 100 krad/h the radiation damage amounts to roughly 5%, the crystal degradation reaches 10-25% [51, 52]. At a dose rate of $\sim$500 krad/h and integrated dose of 1-2 Mrad. Without exceptions, in all cases the loss of resolution is attributed to degradation of the transmission properties of the blocks, and not to the degradation of the photocathode of the PMTs.

The simulated total dose rates for this experiment, calculated in the worst-case scenario of a 6.6 GeV beam energy, amount to 274 rem/h for a 1 μA beam current, 10 cm long cryogenic hydrogen target, and averaged over an angle of 5 to 25 degrees. These dose rates are dominated by (Moeller) electrons. Assuming a 7.5 kG sweep field in the magnet reduces this to 18 rem/h. The dose rates fall rapidly as the angle increases from 5 to 25 degrees, by approximately one order of magnitude. At 5.5 degrees, the dose rates correspond to 400 rem/h (without field) and 50 rem/h (with field), correspondingly.

Given that we have only one kinematics close to this smallest angle (6.3°), and for other kinematics we are at $\sim 8^\circ$ and beyond, the dose rates look acceptable for a 1 μA beam currrent assumption and the proposed sweeping magnet. In addition, we started to prepare custom pre-amplifiers in order to operate the PMTs at lower high voltages, with lower anode currents. More details on the rate simulations and the modified voltage divider design can be found in sections VIII and IX.

F. Detector linearity and efficiency

As described in more detail in section VIII, the main source of background in the detector is low-energy photons. In the worst-case scenario (6.3° [‡]), it is expected to be 200 MHz within the calorimeter acceptance, or on average 200 kHz per module. Of course, the rate of the background is not uniform, and will be a factor of 2-4 higher for the crystals closest to the beam line. The dominant fraction of these photons has energies of about 10 MeV. Note that the critical energy, where ionization and Cherenkov radiation losses are equal, is 8.5 MeV. But, these low-energy photons can still cause pile-up and additional anode current.

The latter is not a real issue, as shown in Fig. 6 which shows that the gain variations can be controlled to better than 1% at up to 1 MHz rates per crystal, with a modified PMT base design as compared to the PRIMEX

[‡] The π^0 scattering angles cover 6.3-24.0 degrees where the angles smaller than 8.6 degrees are only relevant for SIDIS.

experiment. The tests and base modifications are further described in Section VIII. Note that the results for our PRIMEX test setup can also be compared to earlier PRIMEX studies of the PMT gain variation with rate changes induced by different beam conditions in Figure 19. The test results of our new modified active base design show a factor of ∼25 improvement in gain stability over the existing PRIMEX bases (see section IX).

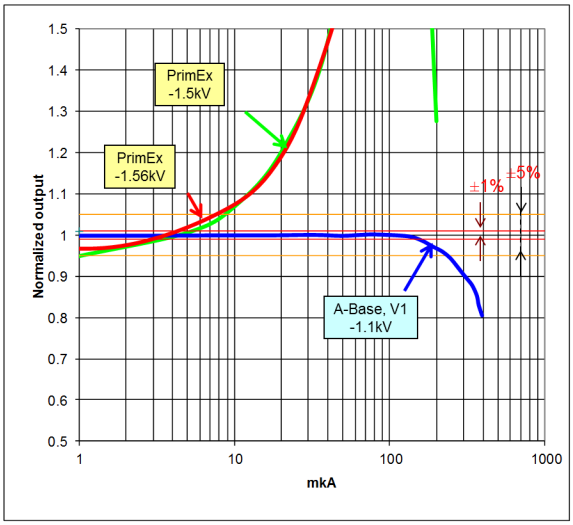

FIG. 6: *Voltage divider gain stability as a function of anode current. The solid red lines denotes stability to 1% and the yellow solid line stability to 5%. The new active base design A-Base, V1 outperforms the PRIMEX bases by a factor of about 25.*

Given that we expect linear gain, the photon background will act solely as an energy baseline shift. First recall that we overdetermine neutral pions both from the measured energy and the decay angle. Second, if we can reduce the background rates, the baseline shift will become less important and is actually small even within a 100 ns gate. Assuming an average photon energy of 10 MeV, the rates mentioned above, and a few crystals firing for each decay photon shower, we would get a baseline shift of less than 10 MeV in a 100 ns gate. This is well within the expected energy resolution of the $PbWO_4$ crystals for photons associated with 2-5.5 GeV neutral pions.

More details on the rate simulations performed will be given in section VIII. Given a maximum background rate of well below 1 MHz per crystal, with the worst case 1 MHz only relevant for the crystal closest to the beam line with the neutral-pion setup at a worst-case minimum angle of 6.3°, we conclude that the gain is stable to about 0.2% for all kinematics and background conditions. As in the PRIMEX experiment, we have included a temperature-stabilization system in the design, hence contributions due to temperature dependences are small, <0.2% (a 0.1°C temperature stability guarantees a 0.5% energy stability for absolute calibration and resolution). Earlier we have shown the combinatoric background to be also small, <1%, where we likely will know this background to a fraction of this. Nonetheless, since the background conditions change with angle, we assigned an uncertainty of about 0.2-0.5%. Lastly, the uncertainty in the geometric acceptance is correlated with the knowledge of survey and actual beam position, but will be well known (<0.1%). Overall, we feel we can achievably assume the π° detection efficiency to be stable to <0.5%.

Note that we have performed radiation tests of the active PMT base in Hall C during Qweak operations. We find no degradation of the base for a radiation dose of 100 kRad equivalent with the full experiment proposed here.

G. Electron Identification and DAQ

We will be detecting electrons with momenta ranging from 1.5 to 5.5 GeV/c in the HMS. The HMS has a lead-glass calorimeter and a heavy-gas atmospheric Čerenkov detector for electron identification. Singles rates are typically constrained in HMS to a level of 0.5 MHz to allow for a detailed understanding of the tracking efficiency. This is not an issue for the present experiment, where HMS singles rates are expected to be less than 2 kHz (see the E12-06-104 proposal [32] for detailed single rates and π/e ratios).

A good pion/electron separation has routinely been achieved in the HMS. The current detector stack of the HMS has been shown to easily achieve e^-/π^- to $\sim 10^3$, with 98% efficiency for electron detection. In this proposal, the π/e ratio is never larger than 130:1. Because of the moderate pion to electron ratios, we require the events of interest to only pass some loose particle identification before generating an HMS trigger. In order to have a high efficiency for electrons, a trigger will be accepted as a true electron if either the gas Čerenkov detector has fired or if the electromagnetic calorimeter has had a large enough signal. This will allow high electron efficiency even if one of the two detectors will have a low efficiency.

The electron trigger (ELREAL) will thus have two components: Electron High (ELHI) and Electron Low (ELLO). ELHI will require a high calorimeter signal, but no gas Čerenkov detector information, and will be composed of a high signal in the "preshower" (PRHI) and a low signal in the full calorimeter (SHLO), in coincidence with scintillator signal (SCIN). Note that the "preshower" for the HMS is simply the first layer of the calorimeter. ELLO will require a gas Čerenkov detector signal. The final HMS trigger (COIN) will be a combination of electron (ELREAL) and sampled pion (PION) triggers, the latter requiring a standard three-out-of-four (3/4) coincidence of the x-y hodoscopes (SCIN), vetoed by a gas Čerenkov detector signal (CER).

The DAQ will record both coincidence triggers between the HMS and the neutral-pion arm, as well as single-arm HMS triggers with inclusive (e,e$'$) and (e,h) events. The latter will not require readout of the pion calorimeter, and the rate can be pre-scaled if necessary. However, given the low inclusive (e,e$'$) rates at a 1 μA beam current, we plan to include all these events in the data stream. This is important for two reasons: i) SIDIS pion multiplicities can be directly formed by taking a ratio of coincidence (e,e$'\pi^\circ$) yields and inclusive (e,e$'$) yields; and ii) the inclusive (e,e$'$) yields will provide an additional normalization for the coincidence data.

In the off-line analysis, we will further use a cut on the coincidence timing between the scattered electron and the π°. Regular cuts on kinematic variables, such as the vertex position, the HMS collimator image, etc., can also be used to reduce any background, although not likely needed for the modest requirements of the proposed experiment. For the exclusive channel, an appropriate cut on missing mass will be included to guarantee exclusivity of the p(e,e$'\pi^\circ$)p events.

V. PROPOSED KINEMATICS

Table II shows the kinematic settings proposed for this experiment. The Q^2-dependence of the separated cross sections and their ratio $R{=}\sigma_L/\sigma_T$ will be examined at several x_B points ranging in z, from 0.4 to 1.0, *i.e.*, the exclusive limit. The kinematics are optimized for the exclusive reaction, but semi-inclusive data can be obtained simultaneously unless stated otherwise. Recall that the exclusive experimental ratio $R{=}\sigma_L/\sigma_T$ is needed for a reliable interpretation of the results from the GPD program. The measurement of the Q^2 dependence at fixed x_B, will provide the first exclusive L/T separated π° data, which is needed for hard-soft factorization studies, a key component in the interpretation of GPDs. For the exclusive limit only, the t' dependence of the cross section will be studied at a fixed value of x_B to constrain the pole to non-pole behavior. The data will be acquired in near-parallel kinematics, which will allow for the separation of the individual cross section components. We have assumed that the HMS can be set to angles ranging between 10.5° and 37°. The minimum angle is the absolute minimum angle attainable with the present HMS, the maximum angle is driven by the planned use of 10 cm

TABLE II: *Kinematic settings for the $p(e,e'\pi^\circ)p$ and $p(e,e'\pi^\circ)X$ measurements. The scattered electron will be detected in the HMS and the pair of γ's from π° decay in the π° detector. The separated σ_L/σ_T ratio will be mapped as a function of z at (small) p_T for each setting. The label p_{π° denotes the exclusive case. The kinematics have been optimized to use the point at Q^2=5 GeV^2 and x_B=0.5 for both the R mapping and the Q^2 dependence studies. Furthermore, the point at Q^2=3.5 GeV^2 and x=0.5 can be used for both the Q^2 and $t-t_{min}$ dependence studies. The two bold-faced entries without a specified $-t_{min}$ value are dedicated to semi-inclusive measurements, to enhance $\Delta\epsilon$, and will only provide limited statistics for the $p(e,e'\pi^\circ)p$ case. The (x,Q^2) = (0.20,2.00) kinematics combinations will also be used for $d(e,e'\pi^\circ)X$ measurements, whereas the (0.20,2.00), (0.30,3.00), (0.40,4.00) and (0.50,5.10) will provide maximal overlap with the approved L/T separated $p(e,e'\pi^\pm)X$ 12-GeV program.*

W (GeV)	Q^2 (GeV^2)	E_e (GeV)	E'_e (GeV)	θ_e (deg)	ϵ	p_{π° (GeV/c)	θ_{π° (deg)	$-t_{min}$ (GeV/c)^2	x
Detailed mapping of $R=\sigma_L/\sigma_T$ at x=0.2, 0.3, 0.4									
2.98	**2.00**	**6.60**	**1.270**	**28.26**	**0.34**	**5.513**	**6.27**		**0.200**
2.98	2.00	8.20	2.821	16.96	0.60	5.304	8.58	0.043	0.200
2.98	2.00	10.80	5.421	10.63	0.79	5.304	10.45	0.043	0.200
2.81	**3.00**	**6.60**	**1.270**	**34.79**	**0.33**	**5.603**	**7.44**		**0.300**
2.81	3.00	8.80	3.422	18.21	0.65	5.269	11.00	0.108	0.300
2.81	3.00	10.90	5.522	12.85	0.79	5.269	12.66	0.108	0.300
2.62	4.00	8.20	2.821	24.07	0.58	5.211	11.67	0.218	0.400
2.62	4.00	10.90	5.521	14.85	0.78	5.211	14.39	0.218	0.400
Scaling study of the Q^2 dependence at fixed x/t (x=0.5, t=0.4)									
2.01	3.50	6.60	3.026	23.72	0.70	3.527	17.42	0.378	0.500
2.01	3.50	10.90	7.120	12.22	0.90	3.527	21.22	0.378	0.500
2.21	4.00	8.20	3.887	20.47	0.73	4.056	16.78	0.384	0.500
2.21	4.00	10.90	6.587	13.59	0.86	4.056	19.19	0.384	0.500
2.45	5.10	8.20	2.716	27.77	0.55	5.222	12.42	0.395	0.500
2.45	5.10	10.90	5.416	16.94	0.77	5.222	15.63	0.395	0.500
Study of the t dependence at fixed x/W									
1.90	2.45	4.40	1.590	34.63	0.56	2.591	16.54	0.312	0.473
1.90	2.45	8.80	5.990	12.41	0.91	2.591	23.94	0.312	0.473
2.10	3.50	6.60	3.026	23.72	0.70	3.527	17.42	0.378	0.500
2.10	3.50	10.90	7.120	12.22	0.90	3.527	21.22	0.378	0.500
2.00	3.80	6.60	2.863	26.02	0.67	3.423	17.52	0.491	0.549
2.00	3.80	10.90	7.163	12.70	0.90	3.423	22.17	0.491	0.549

LH2 (and LD2) targets, for an effective target length as viewed by HMS of 6 cm.

To determine σ_L and σ_T from the data, a minimum of two beam energies is required. To minimize the amplification in the systematic uncertainty, the ϵ settings have been chosen to span $\Delta\epsilon \sim 0.20$ or greater where possible. By adding a third beam energy at Q^2=2.0 and 3.0 GeV^2 a semi-inclusive data set with an enhanced $\Delta\epsilon$ span and significant statistical precision of 1-2% can be obtained. The exclusive rate at these points is small, but the increased $\Delta\epsilon$ range reduces the systematic uncertainty in the L/T separation. This would only add about 5 days ($\sim$ 7%) to the total beam time request.

Figure 7 shows the accessible Q^2-x_B phase space for 12 GeV experiments in Hall C for exclusive and semi-inclusive kinematics. The proposed kinematics allow for a scan of the Q^2-dependence of the cross section at constant x_B while staying above the resonance region. This is important, as our proposed measurement will provide the first data in this region, and allow for reliable tests of the reaction mechanism. As of yet there is no experimental guidance for the L/T character in SIDIS at all, and only model calculations in the exclusive limit.

The $z < 1$ limit data set will concentrate on the more limited kinematical region of $W > 2.4$ GeV (see

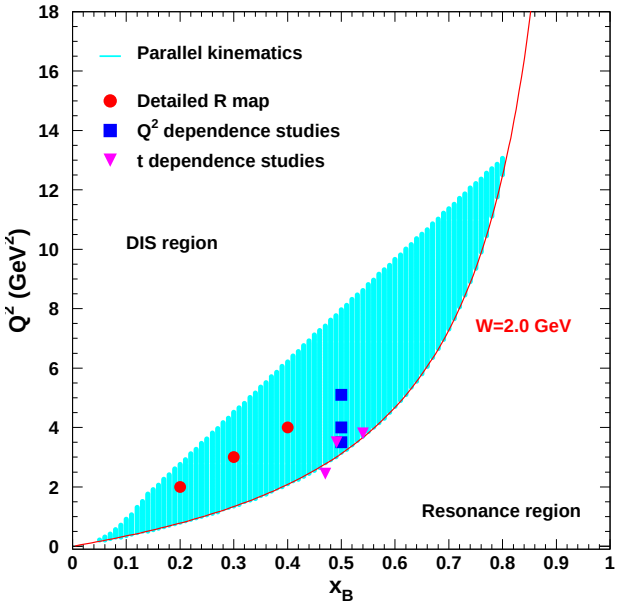

FIG. 7: *Q^2 versus x_B phase space available for L-T separations in Hall C at 11 GeV using the HMS for exclusive and semi-inclusive kinematics. We propose to map the separated ratio σ_L/σ_T ranging in z, from 0.4 to 1.0, the exclusive limit, for p_T (<0.4 GeV/c) at x_B=0.2, 0.3, 0.4, and 0.5, and evaluate the Q^2-dependence and $t-t_{min}$-dependence of the cross sections at fixed x_B=0.5. The kinematics have been optimized to use the point at Q^2=5 GeV^2 and x_B=0.5 for both the R mapping and the Q^2 dependence studies. Furthermore, the point at Q^2=3.5 GeV^2 and x=0.5 can be used for both the Q^2 and $t-t_{min}$ dependence studies. The kinematic reach is limited from below by the requirement on W being above the resonance region and from above by the requirement to maintain a separation of $\Delta\epsilon \sim 0.2$.*

Table II) to maintain a sufficiently high-enough mass of the residual system (M_X or W'). It will provide missing experimental information on the L/T ratio in the semi-inclusive pion electroproduction process, and as such the kinematics were chosen similar as the charged-pion case (E12-06-104), for direct comparisons. Contrary to E12-06-104, however, we do not study the p_T-dependence due to the issues related to averaging out the unknown ϕ modulations with incomplete ϕ coverage (see section IV). The $z = 1$ limit data will provide the first L/T separated exclusive π° cross sections. These L/T separated results will be essential for guiding the interpretation of data from survey experiments with large acceptance detectors, and furthermore, allow for the first studies related to QCD factorization in neutral system and the importance of pole and non-pole contributions in meson production.

The separated ratio $R = \sigma_L/\sigma_T$ will be mapped as a function of z at (x,Q^2) = (0.20,2.00), (0.30, 3.00), (0.40, 4.00), and (0.50, 5.10). The higher energies available at 12 GeV JLab allow for access to a significantly larger range in Q^2 compared to what one could achieve at 6 GeV JLab and, for the first time, with values of W above the resonance region. The access to higher values of W, and thus smaller values of t is important because it provides the first separated exclusive $z \to 1$ π° data in this regime, which will allow for a more reliable interpretation of data from the GPD program. These kinematics are also compatible with the expected flavor decomposition program at 12-GeV JLab, and in particular the companion data for the L/T separated $p(e,e'\pi^\pm)X$ program at 12 GeV in Hall C (*e.g.*, $z < 1$: E12-06-104, $z \to 1$: E12-07-105). To test the equality $R^H_{SIDIS} = R^D_{SIDIS}$, the point at $x = 0.20$ and $Q^2 = 2.00$ GeV^2 will also be taken with a deuterium target.

The Q^2 scan at a fixed value of x_B=0.5 provides the largest lever arm in Q^2=3.5-5.1 GeV^2 above the

resonance region, and will provide reliable L/T separated data for investigations for the onset of $1/Q^n$ scaling in neutral pion systems. One of the goals of the proposed measurement is to extend our knowledge of the relative longitudinal and transverse contributions to the cross section to the largest possible Q^2. Given the constraint imposed by the requirement to keep $-t \ll 1$ (GeV/c)^2, combined with the maximum available beam energy of the upgraded CEBAF and the kinematic reach of the HMS+calorimeter configuration in Hall C, the maximum Q^2 for pseudoscalar meson production is near 10 GeV^2. At this point, $\Delta\epsilon$ is kinematically restricted. We have chosen to limit the maximum Q^2 to 5.1 GeV^2 as the ratio R is effectively unknown, and the projected ratio based on previous charged pion production data predict a rapid increase of the uncertainties at higher values of Q^2. If the data proposed here would indicate that the uncertainties would be acceptable these results can serve as the basis for adding a point in a follow-up measurement. The Q^2 coverage for the proposed measurement is about a factor of two larger than what one could achieve with a 6 GeV configuration at much smaller values of W and $-t$. This facilitates the determination of the Q^2 dependence even if the L/T ratios turn out to be less favorable than predicted by available models. In order to examine the contribution and Q^2 dependence of the interference terms, data will also be acquired to the left and right of the $\vec{q}$.

The measurements at Q^2=2.45, 3.50, and 3.80 GeV^2, which will be carried out for small values of t for each kinematic setting, will provide L/T separated data from which the contributions of σ_L and σ_T can be determined. This would give important information about the role of meson exchange contributions (in the t-channel) and to constrain pole to non-pole behavior. R might be small there, but one should rely on experimental guidance, which does not exist. Indeed, while the model calculations in the shown kinematics have predicted small values of L/T at large Q^2, there is a possibility that actual data would show a value of R more supportive of GPD studies. On the other hand, small values of R could be of interest in the light of recent discussions on transversity GPDs [8, 9] The point at Q^2=2.45 GeV^2 is taken near the resonance region. Together with the proposed kinematics at Q^2=3.5 and 3.8 GeV^2, and data from previous charged pion measurements, this would give powerful constraints on the role of non-pole contributions, which could aid in the reliability of the extraction of the pion form factor at high values of Q^2.

A. Physics Singles Rates and Physics Backgrounds

Singles rates from (e, π°) and (e, e') can result in accidental coincidences which are a source of background for the measurement. However, as compared to the magnetic spectrometer setup planned for various $(e, e'\pi^\pm)$ experiments in Hall C (E12-06-104, E12-07-105, E12-09-011, E12-09-017) the beam current limit of the proposed setup of 1 μA as compared to the more typical >50 μA of the mentioned experiments, with similar length cryogenic targets, implies a negligible accidental coincidence rate of about 2%, which can be easily subtracted.

The singles rate in the HMS is in fact expected to be less than 2 kHz (or 4 kHz for the series of kinematics utilizing LD2 targets). Hence, projected rates for the HMS are low and are well within the operating parameters of previous HMS experiments. In this experiment, the π/e ratio in the HMS is never larger than 130:1, even without reducing this ratio at the hardware trigger level. The electron will be identified using the lead-glass calorimeter in combination with the gas Cherenkov.

The singles rates in the neutral-pion detector are dominated by background. This was simulated and is discussed in detail in section VIII.

We have chosen a liquid hydrogen target with a length of 10 cm. This means that the target end windows will be in the acceptance of the spectrometers (HMS and neutral-pion detection system) in all configurations and background subtractions are necessary. Background events from the target end windows will be measured using "empty" target data. The Hall C empty target consists of two thin Aluminum pieces separated by a length equivalent to the cryogenic target length. However, the empty target is thicker by a factor of 6-7 relative to the target cell walls, a thickness chosen to make the radiation lengths of LH2 (plus windows) and these "empty"

targets about equivalent. The thicker target allows for a more rapid accumulation of counts for these background subtraction measurements.

B. Systematic Uncertainties

The estimated systematic uncertainties for the full $(e, e'\pi^\circ)$ reaction are listed in Table III. These are largely based on previous experience with the HMS+SOS in Hall C and we benefit from the well-understood HMS that determines the (x, Q^2) kinematics allowing for this L/T separation program. In fact, in comparison to recent coincidence measurements in which the electron was detected in the SOS we expect some improvements in the contributions to the systematic uncertainty. For example, the HMS acceptance is much flatter than the SOS acceptance. The neutral-pion acceptance is fully given by geometry and not prone to magnetic field knowledge at all. Tracking efficiency knowledge in the HMS is expected to be excellent at the low rates anticipated in this experiment. In the case of π° detection, the calorimeter performance is expected to be comparable to the one in the PRIMEX-II experiment, with detailed understanding.

TABLE III: *Estimated systematic uncertainties for the π° separated and unseparated cross sections based on previous Hall C experiments. It is important to realize that the HMS is a very well understood magnetic spectrometer which will be used in modest requirements (beyond the momentum), defining the (x, Q^2) kinematics well. The pt-to-pt (scale uncertainties) for radiative corrections and Monte Carlo model are 1.2% (2%) and 0.5% (1%) and should be added in quadrature in the total. The uncorrelated errors between high and low ϵ settings are listed in the first column. The point-to-point uncertainties are amplified by $1/\Delta\epsilon$ in the L-T separation. The scale uncertainties propagate directly into the separated cross sections.*

Source	pt-to-pt (%)	scale (%)
Acceptance	0.4	1.0
Electron PID	<0.1	<0.1
π° efficiency [a]	0.5	1.0
Electron tracking efficiency	0.1	0.5
Charge	0.5	2.0
Target thickness	0.2	0.5
Kinematics	0.4	<0.1
Total (including rad, mod)	1.6	3.4
Total	0.9	2.5

[a] includes combinatoric background, geometric acceptance, etc.

On the other hand, some uncertainties will be larger than, for instance, those projected for the charged-pion L/T separations in electroproduction and the pion form factor measurements at 12 GeV. First of all, the beam current is only 1 μA. We consider adding a tungsten calorimeter to obtain a projected best 1% uncertainty. However, this has not been proven yet, so we assume a 2% scale uncertainty. We assume we can measure the collected beam charge to better than 0.5% relatively. Of course, we note that in the semi-inclusive data analysis only the ratio of $(e, e'\pi^\circ)$ and (e, e') yields is relevant, with absolute beam current knowledge dropping out, whereas for the deep exclusive data analysis we can also elect to normalize on the well-known R_{DIS} values through the inclusive HMS (e,e$'$) yields.

Secondly, we plan to use the HMS momentum up to it's maximum design momentum of 7.3 GeV/c. Data taking at a 6-GeV Jefferson Lab has shown an excellent and stable performance and detailed understanding of this for HMS momentum up to $\sim$ 5.5 GeV/c, but some saturation effects are anticipated in the magnetic performance equivalent to a central momentum of 7.3 GeV/c. The anticipated behavior in the HMS quadrupole

magnets has been mapped through rotating-coil measureents in the early 1990s, but exact implications for the understanding of the HMS optics and acceptance require data. Luckily, the implications are expected to be minor as compared to the magnetic field saturation effects one had to face with the SOS for the earlier 6-GeV precision L/T separation program in Hall C. Nonetheless, even if we only plan to use the HMS at angles below 35° with a modest 10 cm long target, we have retained a 1% scale uncertainty in the understanding of the acceptance of the HMS.

Thirdly, some variation of the gain of the PMTs, and degradation of the $PbWO_4$ channels during the experiment, is anticipated. As shown in Fig. 19 (in section VIII), which is based on actual PRIMEX tests with the $PbWO_4$ crystals, the gain of the $PbWO_4$ crystals stays linear to within 1% up to at least 300 kHz. The reason for the deviation at 1 MHz, is considered to be the nonlinearity of the base. The new HV distribution bases design with built-in pre-amplifiers will allow for operating the PMTs at lower voltage and lower anode currents and allowing to achieve stable gains of better than 1% up to rates of 1 MHz. Nevertheless we have included a projected 1% nonlinearity in gain leading to the projected 1% scale uncertainty of "π° efficiency" in Table III. This is far more conservative than the achieved knowledge from the PRIMEX-II experience. The details of the uncorrelated uncertainty are discussed in section IV F.

Lastly, well-established models for separated pion electroproduction cross sections above the resonace region do not exist, and there will thus be equivalent uncertainty in the radiative correction estimates. This will likely be the largest single systematic uncertainty for the proposed experiment, but can be reduced through further data accumulation for this process with 12-GeV experiments.

VI. PROJECTED ERROR AND TIME ESTIMATE

In preparing the count rate estimate we assume the following: 10-cm liquid hydrogen target thickness and 1 μA electron beam current, HMS solid angle and momentum bite of 5.9 msr and 8%, and calorimeter solid angle of 25 msr. The dominant parameters in the beam time estimate are the ratio of longitudinal to transverse cross sections, $R{=}\sigma_L/\sigma_T$ and the value of $\Delta\epsilon$ between the kinematic settings.

Two measurements at fixed Q^2 and W and different values of ϵ are required to determine σ_L. Recall that a full separation of σ_L and σ_T and knowlege of their magnitudes is needed for the factorization studies in the GPD framework. The uncertainty on σ_L can be derived as follows. Letting $\sigma_1 = \sigma_T + \epsilon_1\sigma_L$ and $\sigma_2 = \sigma_T + \epsilon_2\sigma_L$ then

$$\sigma_L = \frac{1}{\epsilon_1 - \epsilon_2}\left(\sigma_1 - \sigma_2\right). \tag{13}$$

Assuming uncorrelated errors in the measurement of σ_1 and σ_2, one obtains the intermediate expression

$$\frac{\Delta\sigma_L}{\sigma_L} = \frac{1}{\epsilon_1 - \epsilon_2}\frac{1}{\sigma_L}\sqrt{\Delta\sigma_1^2 + \Delta\sigma_2^2}, \tag{14}$$

and by defining $R{=}\sigma_L/\sigma_T$ and $\Delta\sigma/\sigma = \Delta\sigma_i/\sigma_i$ and assuming $\Delta\sigma_1/\sigma 1 = \Delta\sigma_2/\sigma_2$, one obtaines

$$\frac{\Delta\sigma_L}{\sigma_L} = \frac{1}{\epsilon_1 - \epsilon_2}\frac{\Delta\sigma}{\sigma}\sqrt{(1/R + \epsilon_1)^2 + (1/R + \epsilon_2)^2}. \tag{15}$$

Equation 15 demonstrates the error amplification on statistical and uncorrelated systematic uncertainties in σ_L due to the limited ϵ range and R. This equation is important since we will extract all four components of the exclusive cross section. The error amplification depends strongly on the value of R, which is not known experimentally and thus needs to be measured for a reliable extraction of σ_L. The limited ϵ lever arm is the secondary source of error amplification. However, kinematic settings with larger values of $\Delta\epsilon$ are not possible with the given beam energies, and the HMS+calorimeter combination. The total uncorrelated errors between high and low ϵ settings, which are dominated by kinematic and cross section model uncertainties, are listed in

Table III. Given the significant error amplification for uncorrelated errors, the correlated systematic errors of a few percent can effectively be ignored.

The ratio of longitudinal and transverse cross sections is not well known above the resonance region. Theoretical predictions for σ_L in the exclusive $z \to 1$ limit disagree at the $t = t_{min}$ point. However, as shown in Figure 8, in a realistic experimental bin with a width of 0.02 $(\mathrm{GeV/c})^2$, the differences in the model predictions are quite modest, and the average value provides a very reasonable estimate for the count rate. For example, for a bin with Q^2= 4.0 GeV^2 and x_B=0.5, the longitudinal cross section predicted by the VGL/Regge model [53, 54] at the bin center is 6.8x10^{-4} μb/GeV^2, resulting in L-T ratios of ≈0.01. The VGG/GPD model [55] predicts a ratio larger by a factor of about $\sim$ 3 for the same experimental bin, which gives an L-T ratio of ≈0.02. The average of the two is 0.015. This is generally compatible with calculations from the Goloskokov/Kroll (GK) model [8].

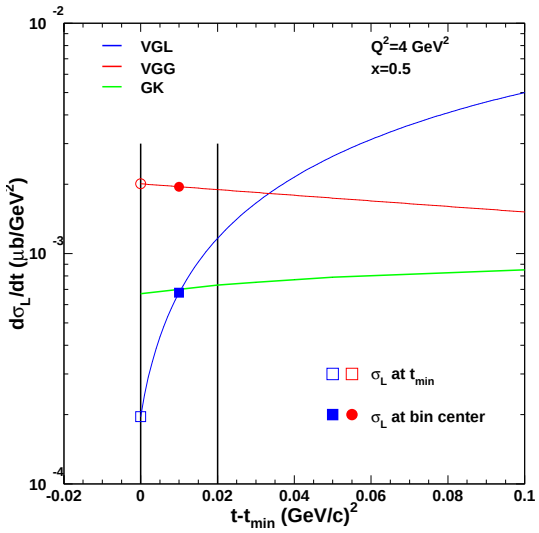

FIG. 8: *The $t - t_{min}$ dependence of σ_L as calculated using the VGL and VGG models. The two vertical bars indicate an experimental bin of width 0.02 $(GeV/c)^2$. The open symbols denote the value of σ_L as calculated at t_{min} and the filled symbols show the value of σ_L as calculated at the center of the bin. Also shown is a calculation of σ_L in the GK model [56].*[b]

To estimate the coincidence N(π°)X rate in the z <1 regime, we used the general Hall C Monte Carlo package SIMC, modified for the semi-inclusive pion electroproduction, following the high-energy expectation of Eq. (10). We used the CTEQ5 next-to-leading-order (NLO) parton distribution functions to parameterize $q(x, Q^2)$ [30], and the fragmentation function parameterization for $D^+_{q\to\pi}(z, Q^2) + D^-_{q\to\pi}(z, Q^2)$, with D^+ (D^-) the favored (unfavored) fragmentation function, from Binnewies *et al.* [31]. The remaining unknowns are the ratio of D^-/D^+, the slope b of the p_T dependence, and the parameters A and B describing the ϕ dependence.

The D^-/D^+ ratio was taken from the HERMES analysis [57] and the b-value were taken as average for $\pi^\pm$ for hydrogen and deuterium targets extracted in the Hall C data [58] ($b \approx 4.9$). We assumed the parameters A and B to be zero for the rate estimates, which is not a major assumption. We run SIMC for π^+ and π^- and took π° as an average of $\pi^\pm$ ($\sigma_{\pi^\circ} = \frac{1}{2}(\sigma_{\pi^+} + \sigma_{\pi^-})$).

[‡] GK note that the results of their model calculations for these kinematics may not be accurate as the model is optimized for small skewness (less than about 0.1) [56].

Lastly, we assumed that the rates for $z > 0.70$ were identical to those at $z = 0.70$, to mimic the fact that the high-z cross sections are underestimated in the E00-108 experiment.

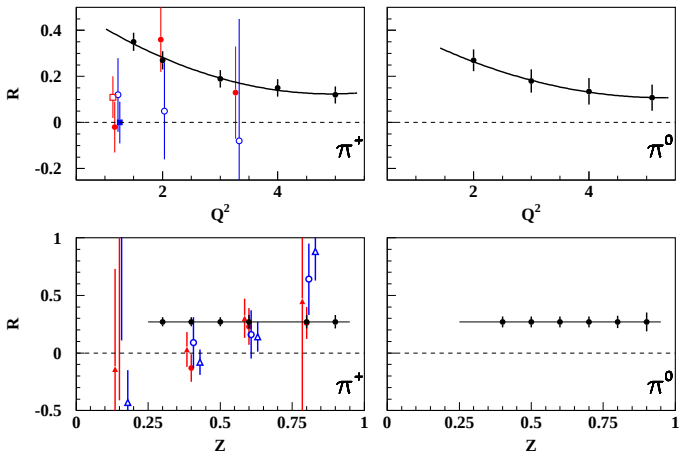

FIG. 9: *The ratio of longitudinal to transverse cross section (R=σ_L/σ_T) for charged and neutral pion production as a function of Q^2 (top panels) and z (bottom panels). The bottom panel on the right represents one Q^2 value and the top panel on the right represents one z bin. The values for R from earlier 70s Cornell experiments [26–28] are shown along with the projected uncertainties of the proposed measurement (black/blue). Different symbols correspond to different values of W^2. The solid curve is the expectation of R from Deep-Inelastic-Scattering.*

To illustrate the sensitivity of the measurement, Figure 9 shows the projected uncertainties of the Q^2 and z dependences of R=σ_L/σ_T. We assume 5,000 counts per z bin (with width of 0.1). The top right panel represents one z bin and the bottom right panel represents one Q^2 bin for π° production. For each of these Q^2 points (and the Q^2 scan, which is not shown in this figure) data will be taken in a range of z between 0.4 and 1.0. The left column shows data and projections for the charged 12 GeV pion experiment E12-06-104. The location of all points is based on deep inelastic scattering.

The exclusive experimental ratio R=σ_L/σ_T is needed for a reliable interpretation of the results from the GPD program. However, there are currently no L/T separated π° data available above the resonance region. This emphasizes the need to experimentally determine the longitudinal and transverse cross sections (or put a boundary on their values). For the rate estimates in this limit, there is no experimental guidance as parameterizations based on previous neutral pion production data are limited to a region outside of our proposed kinematics. One thus has to rely on models like the VGL Regge model by Vanderhaeghen, Guidal, and Laget [53, 54], which provides a globally good description of the longitudinal π^+ cross section for the available data over an extended range of $-t$. Another model that was previously used successfully to describe our separated charged pion cross section data at JLab 6 GeV is the VGG/GPD model by Vanderhaeghen, Guidal, and Guichon [55]. Both models provide a good description of σ_L and a conservative Ansatz for σ_T. As discussed above, both models seem consistent at the level needed to provide reasonable rate estimates. Several other theoretical efforts [8, 15, 19, 59–61] have also recently become available, in particular to improve the description of σ_T in the VGL/Regge model. For σ_L the models mentioned above do not differ significantly. For the rate estimation we have thus used the average value of the VGL/Regge and VGG/GPD cross section predictions for σ_L, and the VGL/Regge predictions for σ_T, σ_{LT} and σ_{TT}. The average of VGL and VGG is compatible with calculations from the model by Goloskokov and Kroll [8, 56]. Figure 10 illustrates the projected uncertainties for R_{excl} at x=0.2, 0.3, and 0.4 assuming roughly 1000 exclusive events per ϵ setting.

For estimating the uncertainty on the cross sectio ratio, we project an uncorrelated point-to-point uncertainty of 1.6% as shown in Table III. For statistical uncertainties of 1-2%, the uncertainty in ΔR will thus be

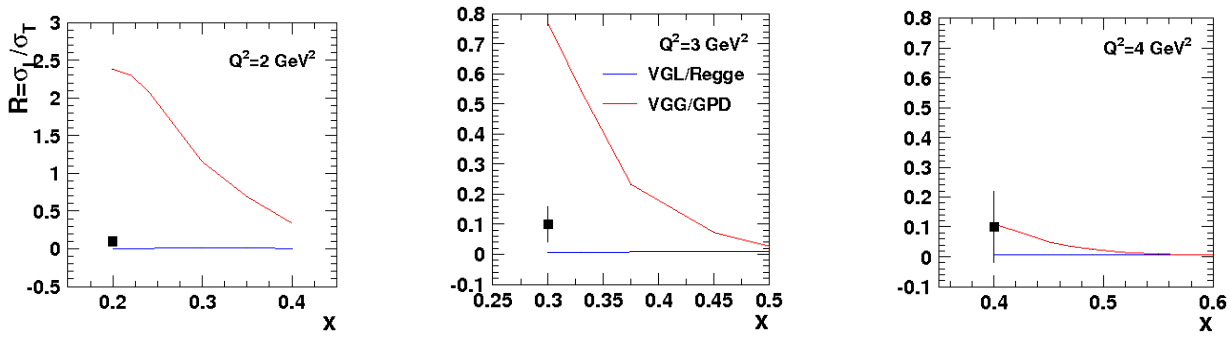

(a) (b) (c)

FIG. 10: *The x dependence of the separated cross section ratio, $R=\sigma_L/\sigma_T$, in the exclusive limit $z \to 1$. The error bars denote the uncertainty as calculated from the statistics and the systematic estimate from Table III and the $\Delta\epsilon$ ranges from Table II. We assume roughly 1000 exclusive events per ϵ setting. The proposed points (filled symbols) were placed arbitrarily at 0.1. Also shown are calculations based on the VGL/Regge model [53, 54] (blue solid) and the VGG/GPD model (red solid) [55].*

in the 0.05-0.10 range, varying with the value of ϵ. For instance, if R would be 0.2 we can measure it to about 25-50%, again depending on which kinematics this was, with which ϵ range. L/T separations are driven by the point-to-point uncorrelated uncertainties. Thus, to get any information on R, and even more so for the extracted longitudinal cross section, small uncorrelated point-to-point uncertainties are essential. Given that there are currently no data for these kinematics, one can argue about the predictive power of the existing models and the implications for the error estimates, but ultimately this issue can only be resolved by actually performing the measurement.

The separated ratio $R = \sigma_L/\sigma_T$ will be mapped as a function of z at (x,Q^2) = (0.20,2.00), (0.30, 3.00), (0.40, 4.00), and (0.50, 5.10). The higher energies available at 12 GeV JLab allow for access to a significantly larger range in Q^2 compared to what one could achieve at 6 GeV JLab, and for the first time with values of W above the resonance region. The access to higher values of W (smaller values of t) is important because it provides the first separated π° data in this regime, which will allow for a more reliable interpretation of results from the GPD program in the exclusive $z \to 1$ limit. The kinematics are compatible with the flavor decomposition program at 12-GeV JLab, and in particular the companion data for the L/T separated $p(e,e'\pi^\pm)X$ program at 12 GeV in Hall C (*e.g.*, $z < 1$: E12-06-104, $z \to 1$: E12-07-105). To test the equality $R^H_{SIDIS} = R^D_{SIDIS}$, the point at $x = 0.20$ and $Q^2 = 2.00$ GeV^2 will also be taken with a deuterium target.

The L/T separated data at a fixed value of x_B=0.5 will be used for tests of the onset of the $1/Q^n$ scaling in neutral pion systems. To illustrate the sensitivity of the experiment, the projected uncertainties of the Q^2 dependence of the π° longitudinal and transverse cross section ratio is shown in Figure 11. The symbols indicate the proposed π° measurement. We assume at least 1,000 good events for each ϵ setting to determine the Q^2 dependence of the reaction. The uncertainties on the proposed points have been estimated assuming a systematic uncertainty of 1.6% in the unseparated cross section, and correlated uncertainties as listed in Table III. The projected uncertainty in the fitting exponent in the Q^n dependence is 0.9. This measurement will provide the first determination of the Q^2 dependence in π° production.

The t' scan data at Q^2=2.45, 3.50, and 3.80 GeV^2 in the proposed measurement will provide L/T separated data above the resonance region to determine the contributions of pole and non-pole contributions. These data will provide important information about non-pole contributions to σ_L in charged pion production. Figure 12 illustrates the projected uncertainties, which have been estimated average value of the VGL/Regge and VGG/GPD cross section predictions for σ_L, and the VGL/Regge predictions for σ_T, σ_{LT} and σ_{TT}, assuming a systematic uncertainty of 1.6% in the unseparated cross section, and correlated uncertainties as listed in Table III.

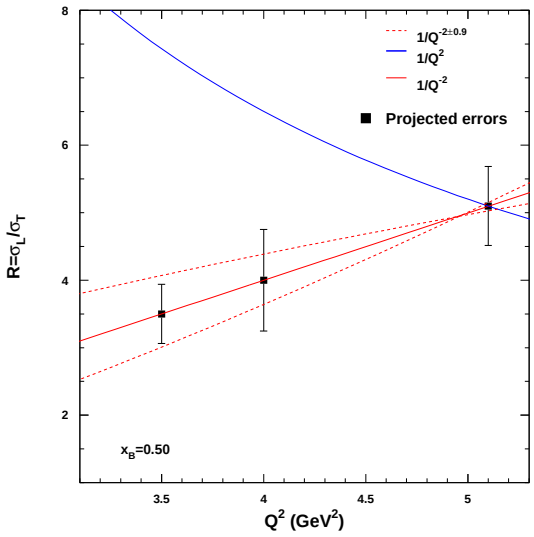

FIG. 11: *Projected uncertainties for the Q^2 dependence of σ_L/σ_T at x_B=0.5. The points are plotted assuming the hard scattering expectation $R\ 1/Q^{-2}$. The solid blue line assumes the hard scattering prediction for σ_L, but that σ_T scales as in DIS. The error bars were calculated using the systematic uncertainties listed in Table III and the $\Delta\epsilon$ values from Table II.*

If the data indicate that the non-pole contributions are smaller than expected, this will allow for determining the pion form factor to values of $Q^2 \sim 10$ GeV^2.

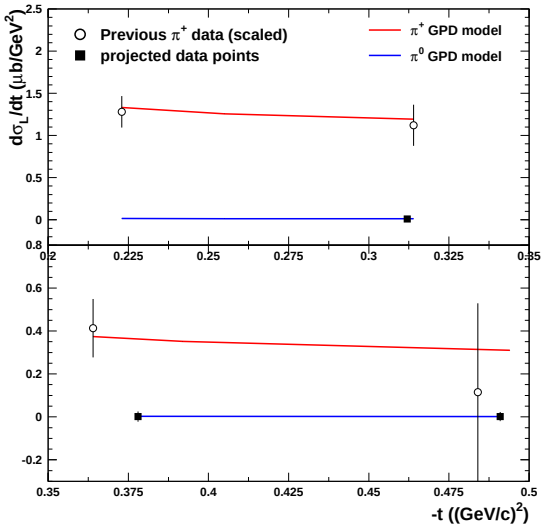

FIG. 12: *Projected uncertainties for the t dependence of σ_L at fixed W/x, in the limit $z \to 1$. The proposed points (filled symbols) were placed arbitrarily at 0.01. The error bars denote the uncertainty as calculated using the systematic uncertainties listed in Table III and a value of R in equation 15 as predicted by the average of the VGL and VGG models. The open symbols are earlier charged pion data. Also shown are curves based on the VGG/GPD model for charged (red solid) and neutral (blue solid) pions.*

TABLE IV: *Beam time estimates for the $p(e,e'\pi^\circ)X$ measurement assuming 1 μA on a 10-cm LH2 target. The kinematics have been optimized to use the Q^2=5.1 GeV^2 point for both the R mapping and the Q^2 scan at x=0.5. The Q^2=3.5 GeV^2 point was optimized for both the Q^2 and t dependence studies. The LD2 data will be taken at the x=0.2 and 0.3 settings of the R mapping in Q^2.*

Q^2 (GeV^2)	x_B	ϵ	LH_2 hours	Dummy hours	Overhead (hours)	Total (hours)
2.00	0.20	0.60	42	6	2	50
2.00	0.20	0.79	8	1	2	11
3.00	0.30	0.65	151	23	2	176
3.00	0.30	0.79	66	10	2	78
4.00	0.40	0.58	100	15	2	117
4.00	0.40	0.78	41	6	2	49
Subtotal R mapping in Q^2			408	61	12	481 (20 days)
3.50	0.500	0.70	48	7	2	57
3.50	0.500	0.90	15	2	2	19
4.00	0.500	0.73	63	10	2	75
4.00	0.500	0.86	33	5	2	40
5.10	0.500	0.55	210	32	2	244
5.10	0.500	0.77	90	14	2	106
Subtotal Q^2 scan at x_B=0.5			459	70	12	541 (23 days)
2.45	0.50	0.56	150	23	2	175
2.45	0.50	0.91	72	11	2	85
3.80	0.50	0.67	21	3	2	26
3.80	0.50	0.90	10	2	2	14
Subtotal t scan at x_B=0.5			253	39	8	300 (13 days)
LD2			51		2	53 (2 days)
SIDIS enhanced $\Delta\epsilon$			103	16	4	123 (5 days)
Subtotals						1498
Calibrations						48
Calorimeter curing						72
beam energy changes						32
Total						1650 (69 days)

The resulting beam time estimate is listed in Table IV. Our total time request is for 55 days of exclusive and 7 additional days for semi-inclusive data, but additional time ($\approx$ 7 days) will be needed for calibration purposes, calorimeter curing, and beam energy changes. Configuration changes have already been included in the time estimate in Table IV. For example:

- $H(e,e')$p elastic data and normalization checks $\approx$ 16 hours
- Spectrometer calibrations $\approx$ 16 hours
- Optics calibrations requiring $\approx$ 16 hours
- Energy and pass changes $\approx$ 32 hours
- Calorimeter calibrations $\approx$ 72 hours

The experiment will require 3 different linac energies and at one of them 2 pass changes. We assume an additional 8 hours overhead for each linac energy change and 4 hours for each pass change. The experiment will make use

of the HMS spectrometer in Hall C, a new calorimeter for π° detection, and require a 10-cm cryogenic hydrogen target.

VII. SUMMARY

In summary, we propose to use the well-known HMS spectrometer and a gereneral-purpose, rotatable neutral-pion detection system in Hall C to perform *simultaneous* L/T separations of the (deep) exclusive $p(e,e'\pi^\circ)p$ and the semi-inclusive $p(e,e'\pi^\circ)X$ reactions. The data will be mapped over a range of x and Q^2, at all settings extending from elasticity z of 0.4 to the exclusive limit, $z = 1$. The data will provide additional information about the $-t$ dependence of the exclusive $p(e,e'\pi^\circ)p$ reaction, and the p_T dependence of the $p(e,e'\pi^\circ)X$ reaction, for $p_T < 0.4$ GeV/c.

These will provide the first high-quality L/T separations for these channels in the intermediate Q^2 region, and be powerful tools to constrain our understanding of the dynamics of these reactions towards a partonic description. The data will go hand-in-hand with the approved L/T separations for charged-pion and charged-kaon electroproduction experiments in Hall C, both in the exclusive and semi-inclusive scattering domains, and be required for the multi-Hall planned 12-GeV program for scalar meson production that focus both on Generalized Parton Distributions and imaging, and on Transverse Momentum Dependent Parton Distributions and corresponding angular asymmetries. The combined data will provide a powerful tool to shed light on our understanding of the parton dynamics underlying these reactions.

We will construct a general-purpose neutral-pion detection system in Hall C, cantelevered off the SHMS carriage and thus remotely rotatable (over an angular range between 6° and 29°), and require 70 days of beam time to map the ratio $R = \sigma_L/\sigma_T$ for the exclusive $p(e,e'\pi^\circ)p$ and the semi-inclusive $p(e,e'\pi^\circ)X$ reactions over a kinematics phase space of relevance for the JLab 12-GeV physics program.

VIII. ELECTROMAGNETIC BACKGROUND SIMULATIONS

We will use the inner $PbWO_4$ high-resolution part of the Hybrid Electromagnetic Calorimeter (HYCAL) [62] for the detection of the photon-pairs from π° decay. The HYCAL calorimeter has previously been successfully used in JLab's Hall B PRIMEX and PRIMEX-II experiments, to precisely measure the neutral pion's lifetime. Energy and coordinate resolutions of $\sigma/E = 1.3\%$ and σ_x ~1.28-2.10 mm have been achieved at a neutral-pion energy of 5 GeV, comparable to the exclusive case of the proposed experiment.

Special attention must be paid to the calorimeter radiation damage. For the envisioned small angles of this experiment, the neutral-pion detector will operate at high rates, and associated high radiation dose. In such conditions, the $PbWO_4$ crystals can accumulate doses that would damage their transmission properties. This would result in a loss of energy resolution of the calorimeter, which in turn worsens the missing mass resolution. The actual radiation damage is determined by both the instantaneous dose rate and the integrated doses. Within an electron scattering environment, the generated radiation doses absorbed by the calorimeter crystals are dominated at angles less than 10° by Moeller electrons (and related Bremsstrahlung).

For $PbWO_4$ blocks radiation effects have been tested in HEPI (Protvino, Russia), at Brookhaven National Laboratory, and at CERN. A radiation hardness study of $PbWO_4$ crystal blocks intended for the BTeV experiment [64] showed that the radiation damage indeed depends on the dose rate (Rad/unit of time) for crystals irradiated by pure, intense high energy electron and hadron beams as well as a mixture of hadrons, neutrons and gammas. Dedicated radiation dose studies showed that the $PbWO_4$ crystals only degradate by 2-3% for low dose rates, 15-20 krad/hr or less instantaneous rates and below 10 krad integrated doses [51]. Radiation damage dramatically increases at high doses. For example, if at dose rate 100 krad/hr the radiation damage amounts to $\sim$ 5%, the crystal degradation reached 10-25% at instantaneous dose rates of $\sim$ 500 krad/hr and integrated doses of 1-2 Mrad [51, 52]. Without exceptions, in all cases the loss of resolution is attributed to degradation of the transmission properties of the crystals, and not to the degradation of the photocathode of the PMTs.

The major sources contributing to the dose in this experiment are the target-induced rates themselves, and apertures of the beam line where large-thickness materials such as vacuum flanges are at the closest (critical) distance from the beam. The incident beam will scatter in the target, and (multiple) scattering products will hit such narrow sections first. Subsequently, they will locally deposit almost their full energy in the beam pipe in the form of an electro-magnetic cascade, irradiating a forward angular cone. To minimize this background, a conical or telescopic design of the initial portion of the beam exit line would be useful. This requirement routinely conflicts with the physics need to put the active detectors or spectrometers at forward angles.

Obviously, it is optimal to make the opening or critical angle for the beam exiting the target/scattering chamber region as large as possible. For instance, if the critical angle was increased to that determined by the two-feet diameter last section of the beam exit line far downstream, a few degrees, then the main cone of scattered electrons would remain inside the vacuum pipe until well beyond the envisioned active detector and detector background, as well as the general background in the Hall, will be significantly decreased. The present "standard" critical angle for the Hall C configuration is about one degrees, inducing the need for additional lead shielding between the beam line and the detector. In that sense, it can be much more efficient to use a second beam pipe with increase flare or critical angle. We plan to design such beam pipe for the bulk of the proposed experiments, as only a few kinematics truly drive the small-angle detection.

The background rates and the π° detector radiation doses for the proposed experiment (for now without the effect of the sweeping magnet included) have been calculated by Pavel Degtiarenko [65]. The various particle rates as a function of angle and particle energy as induced by the interaction of a 6.6 GeV electron beam and a 10 cm liquid hydrogen target are shown in Figs. 13 and 14, for photons, positrons, electrons and positively-charged pions, as examples. These rates are normalized for a 1 μA beam current and a 10 msr solid angle detector.

Given the strong angular dependence of background rates, we only show the rates and radiation doses for angles smaller than 20° in Figs. 13 and 14. Rates at larger angles are completely negligible compared to this.

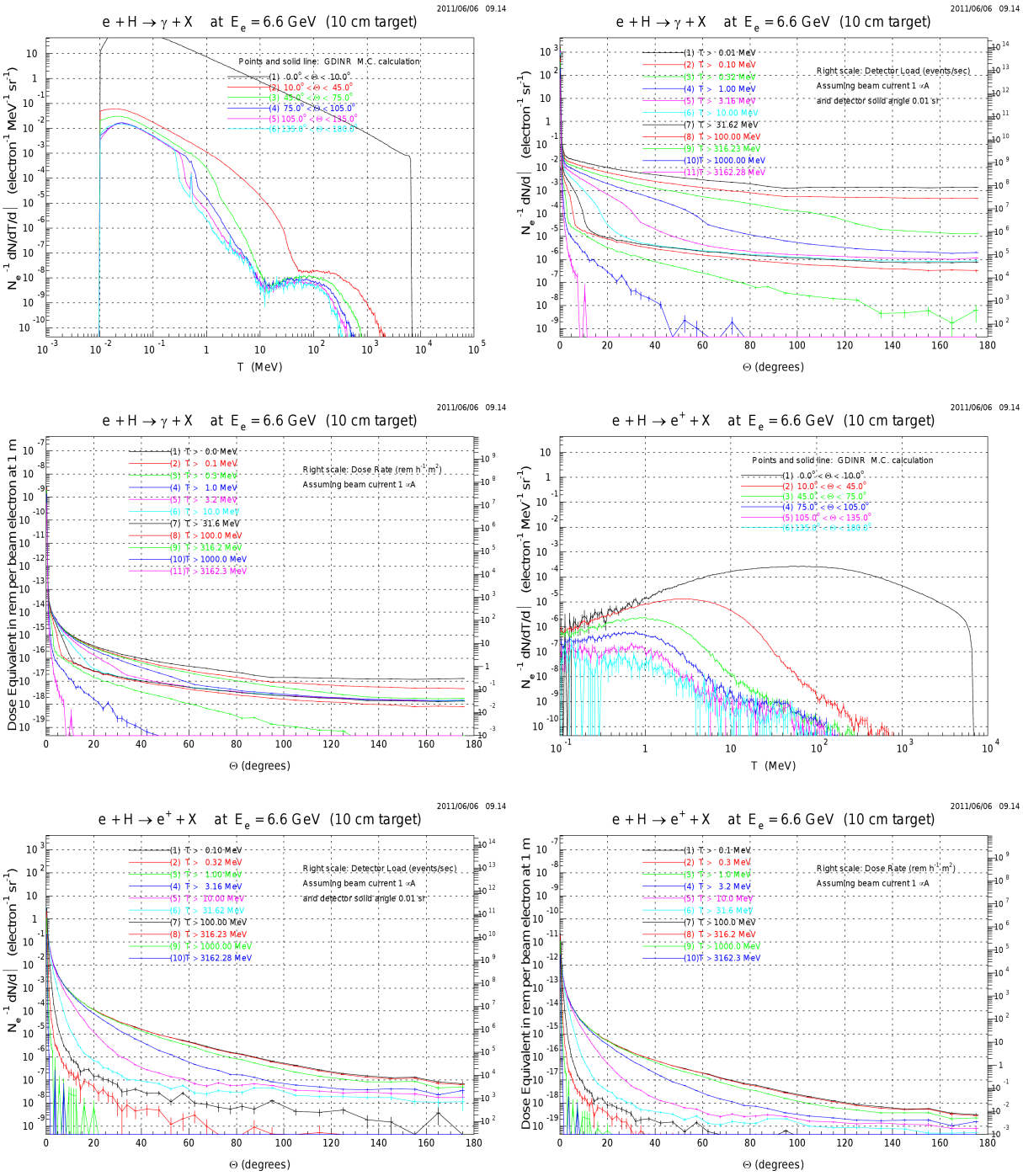

FIG. 13: Expected particle background rates and the radiation dose as seen by a 10 msr π° detector for photons and positrons, assuming a beam energy of 6.6 GeV, a beam current of 1 μA, and a 10 cm LH2 target.

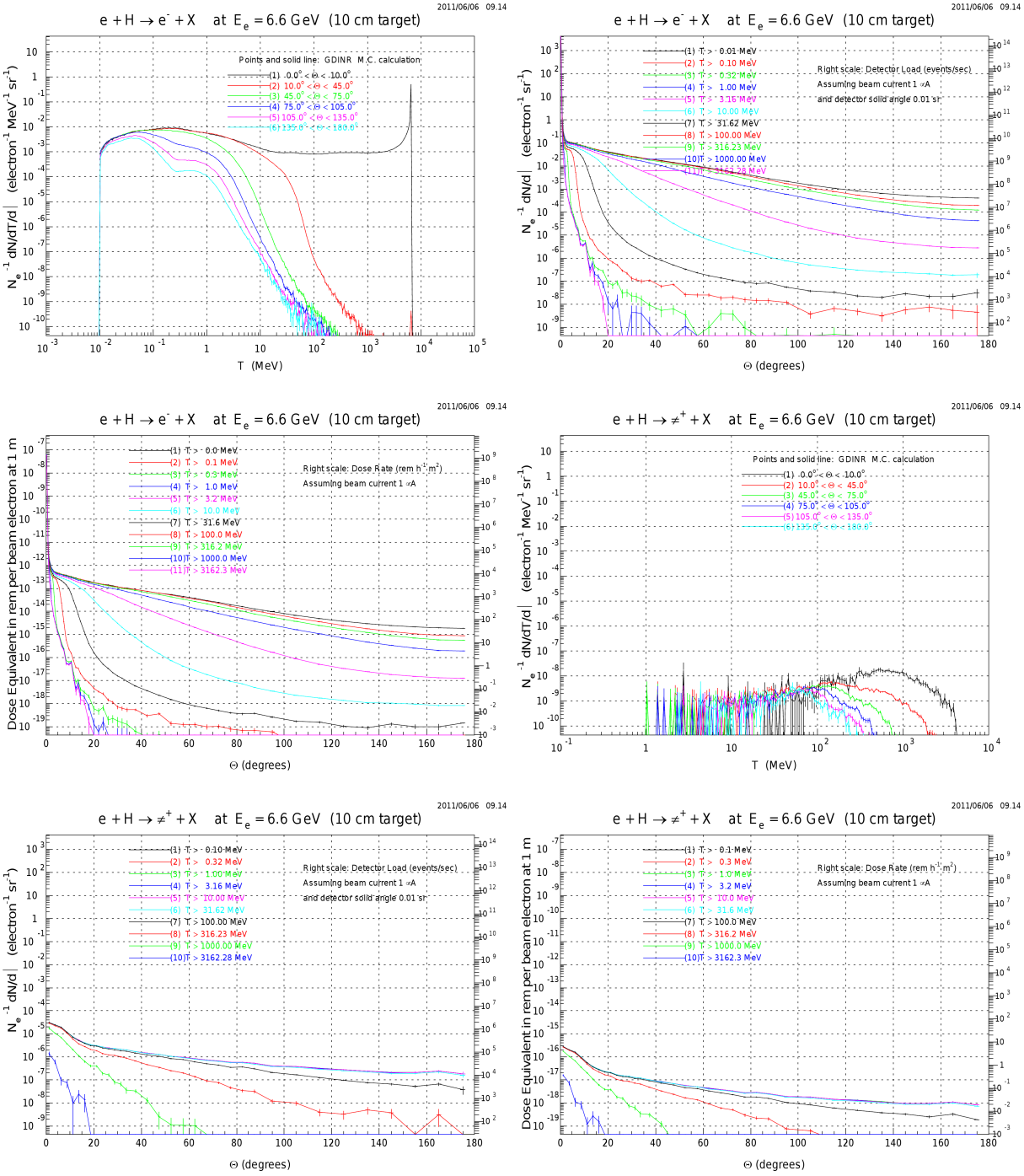

FIG. 14: Expected particle background rates and the radiation dose as seen by a 10 msr π° detector for positrons and π^+, assuming a beam energy of 6.6 GeV, a beam current of 1 μA, and a 10 cm LH2 target.

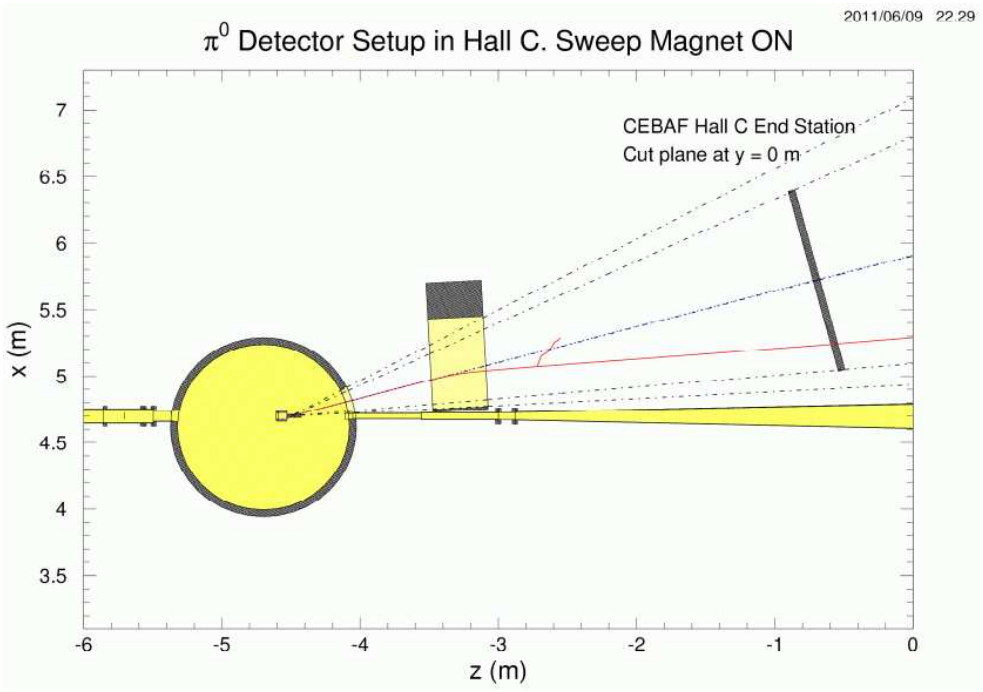

FIG. 15: The schematic layout of the sweep magnet.

This strong angular dependence is further highlighted in Table V, which shows the estimated rates (events per second) for photons, electrons and positrons for a detector with solid angle of 10 msr positioned at 3.5, 6.0 and 8.5 degrees, respectively.

Taking into account that in this experiment we plan to use an ∼1000-channel lead-tungsten calorimeter with a solid angle of about 25 msr, the particle rates will be higher by factor of 2.5, resulting in a rate per crystal of over 2 MHz for angles ≤6 degrees, with the major fraction of the rates produced by Moeller electrons. It is obvious that the use of a magnet to sweep these electrons is essential.

Fig. 15 shows the layout of the experiment as used in the simulations. The layout includes the 10 cm LH2 target located inside the 12-GeV-compatible existing Hall C scattering chamber. The mechanical dimensions of the HB magnet with its bore are used to indicate the yoke and position of the sweeping magnet, bending electrons inwards (towards smaller angles). Here, a 7.5 kG magnetic field is simulated, corresponding to 0.3 Tm. The front face of the detector is at a distance of 4 meter from the target, and covers in this layout an angular range between 5 and 25 degrees. The black dashed-dotted lines correspond to angles of 3, 5, 15, 25 and 28 degrees, respectively. The red track shows the trajectory of a 500 MeV electron emitted at an angle of 15 degrees. We note that the 0.2-0.3 Tm design requirement of the sweeping magnet is driven by guaranteeing

Particle	3.5°	6.0°	8.5°
Electron	3×10^9	6×10^8	6×10^6
Positron	6×10^6	6×10^5	2×10^5
Photon	4×10^8	2×10^8	1×10^8
Total	3.4×10^9	8×10^8	1×10^8

TABLE V: Particle rate (event/sec) for a detector with solid angle of 10 msr located at an angle of 3.5, 6.0 and 8.5 degrees, respectively. These rates assume a beam energy of 6.6 GeV, a beam current of 1 μA, a 10 cm long LH2 target, and no sweeping magnet.

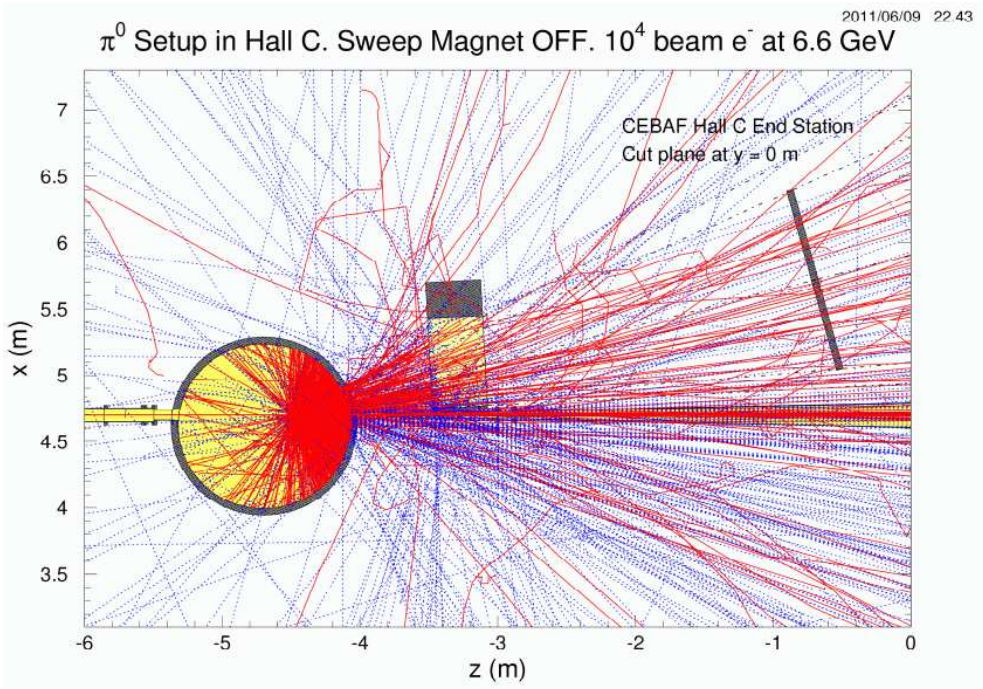

FIG. 16: Simulated trajectories for 10000 beam electrons with an energy of 6.6 GeV, with the sweeping magnet OFF.

sufficient bending power to sweep away up to 300 MeV electrons. This has a tremendous impact on the particle rates shown earlier in Fig. 14 (top right panel).

Figs. 16 and Fig. 17 further show simulated trajectories for 10000 beam-electrons with an energy 6.6 GeV, with the sweep magnetic field "OFF" and "ON", respectively. Blue and red tracks correspond to photons and charged particles, respectively, and the "cleaning" effect of the sweeping magnet can be readily seen.

To quantify the effects of the sweeping magnet further, the results of the dose rate calculations (in rem/hr) for a 1μA beam current and a 6.6 GeV beam energy, with a 7.5 kG magnetic field (0.3 Tm) OFF and ON are presented in Table VI. We note that the presented results are *averaged* over the 5-25° detector front face. The dose rates fall rapidly as the angle increases from 5 to 25 degrees, by approximately by one order of magnitude. At 5.5 degrees the dose rates correspond to ∼400 rem/hr for the field OFF, and ∼50 rem/hr for the field ON configuration. The latter looks certainly acceptable. We further illustrate the results of detector count rates

	Magnet OFF	Magnet ON
Photon dose rate	3.03±0.03	2.81±0.03
Positron dose rate	5.43±0.13	3.75±0.11
Electron dose rate	265.23±0.95	11.48±0.23
Total dose rate	273.69±0.96	18.04±0.26

TABLE VI: Simulated dose rate (rem/hr) for a 1 μA beam current and a 6.6 GeV beam energy, with a 7.5 kG (0.3 Tm) magnetic field OFF and ON. The errors are purely statistical and somewhat underestimated as a Gaussian approximation has been used for a distribution that is significantly non-Gaussian.

as simulated with the well-calibrated GEANT3 code used for successful execution of all JLab experiments in Fig. 18. The six panels correspond to three different energy thresholds each, with the sweeping magnet both ON (left panels) and OFF (right panels). The flux is in the Hz/cm^2 range at the front face of the neutral-pion detector and is a function of the position horizontally along the detector, and away from the beam line. The bin

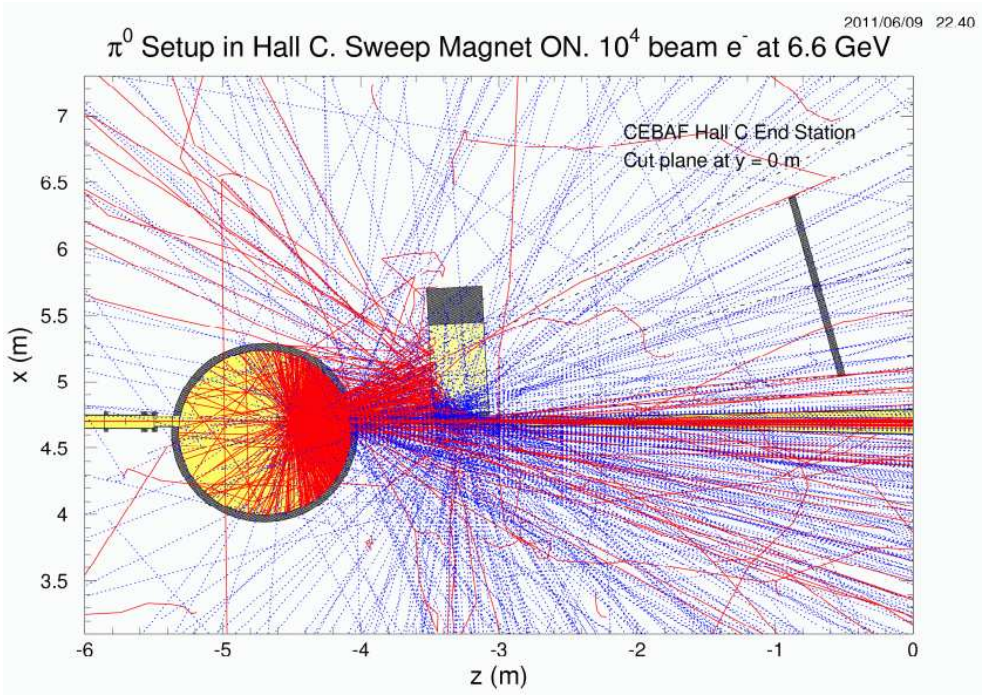

FIG. 17: Same as Fig. 17 with the magnetic field ON.

sizes correspond roughly to steps of one degree in the scattering angle.

With the magnetic field added, the dominant source of the background rates now become photons with an energy above 10 MeV and electrons with an energy above 100 MeV. As one would have anticipated, the use of a relatively simple sweeping magnet will dramatically reduce the (Moeller) electron rates. At the smallest angles foreseen, the rate of photons with energies $E_\gamma > 10$ MeV is $N_\gamma \sim 3 \times 10^5$ Hz/cm^2. For $PbWO_4$ crystals with dimension of 2.05×2.05 cm^2, the photon rate per crystal is $\sim 1.2 \times 10^6$ Hz. The electron rates with energy E_e >100 MeV is $N_e \sim 6{\times}10^5$ Hz/cm^2, or $\sim 2.5{\times}10^6$ Hz/crystal without sweeping field, and drops to $N_e \sim 5{\times}10^4$ Hz/cm^2, or $N_e \sim 2 \times 10^5$ with sweeping field. This shows the sweeping magnet has, as designed, also still quite some impact on electrons with energy above 100 MeV.

Studies show that the gain changes at the few-percent level for a dose rate < 1 Rad/hr. Two types of $PbWO_4$ crystals, SIC and BTCP, showed opposite behavior in the detector response above dose rates equivalent to 4 GeV electrons at ∼ 50 kHz, in early tests of the PRIMEX collaboration [66]. This behavior could be caused by three effects:

- change of scintillation mechanism in the crystals;
- change in the light transmission in the crystals;
- change in the PMT gain due to rate variations.

The results of the PRIMEX studies of the PMT gain variation with rate are presented in Fig. 19.

The overall variation of the measured signals relative to their values at modest 5 kHz rates (for 4 GeV electrons) was found to be modest, ±1%, for rates ranging up to about 10^5 Hz. Such a high rate requires a PMT with a fast response, operated at low gain and low anode current. We consider the construction and use of custom pre-amplifiers to allow operation of the PMTs at lower high voltages, and compensate the gain.

Given that the loss of amplitude is considered due to degradation of the transmission properties of the blocks, and not to degradation of the photo-cathode of the PMTs, it is possible to cure any radiation damage

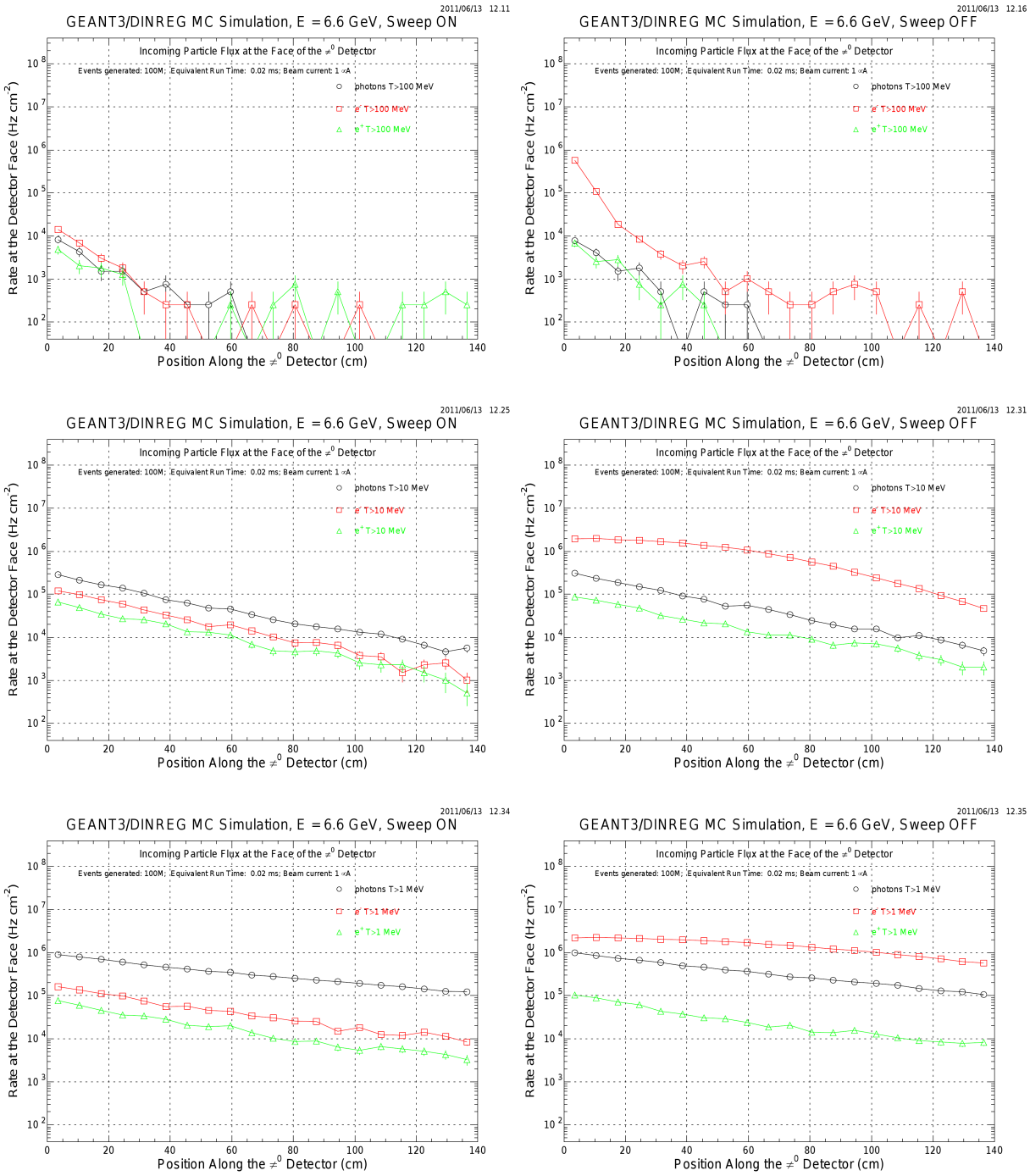

FIG. 18: Simulated flux of the particles (in Hz/cm^2) at the face of the detector as a function of the position, at three energy thresholds and with the sweeping magnet ON (left) and OFF (right).

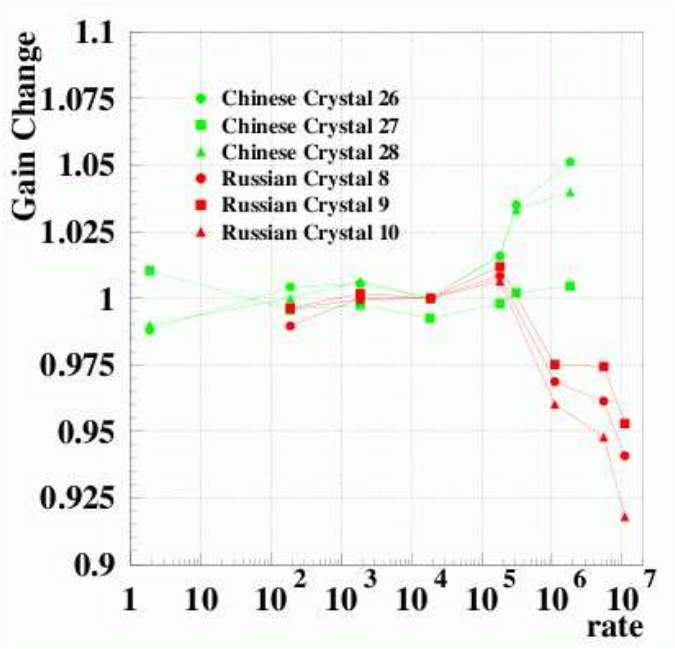

FIG. 19: The variation of the PMT gain of two different type of $PbWO_4$ crystals as tested for the PRIMEX apparatus, as a function of the rate induced in a low-current electron beam test.

by exposing the $PbWO_4$ crystals to near UV blue light. A continuous monitoring of the crystal performance through the π° mass reconstruction from $H(e, e'\pi^\circ)X$ events can be considered, and we may as a result do 2-3 curing cycles during this experiment, each taking 1 day of time. Therefore, we have included three additional days of curing to the beam time request. Based upon detailed further background simulations for the final run plan of this proposed experiment, we can alternatively use (part of) this time to change for a beam pipe of larger critical angle for those angle-configurations compatible with such a setup.

Lastly, we may consider calibration of the calorimeter via elastic $H(e, e'p)$ measurements, which could simultaneously provide for a geometrical survey of the relative positioning of spectrometer and calorimeter.

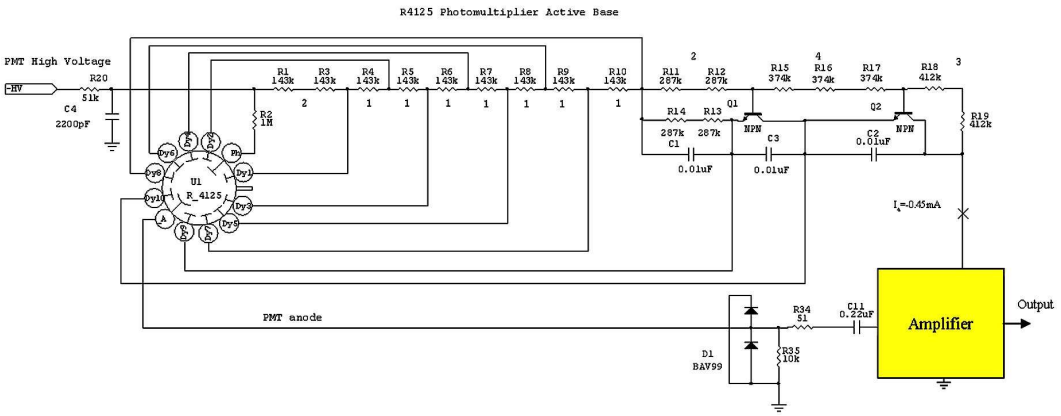

FIG. 20: *R4125 Photomultiplier tube active base circuit diagram. Two (Q1, Q2) high voltage transistors are added to the last two dynode power connection nodes.*

IX. TEST RESULTS FOR R4125 PHOTOMULTIPLIER TUBES WITH ACTIVE BASES

Since the last PAC38 we have redesigned the R4125 photomultiplier used for the $PbWO_4$ crystal readout during the PrimEx experiment to have an active base. Here, the amplifier was powered from a high-voltage division chain. An initial "V0" base was tested with using a 5 mm^3 cube of Pr:LuAG scintillator to simulate a light pulse wave form similar to that of a $PbWO_4$ crystal, albeit with a factor of 200 more light output. This setup allows to simulate light corresponding to a few hundred of MeV energy deposited in $PbWO_4$ using common gamma sources. The setup was equipped with an LED diode to map the gain dependence as function of anode current. Results were encouraging, and a large gain factor ($\sim$ 25) was established with respect to the Primex existing base.

Nonetheless, these test results of the first prototype showed similar problem as the original PRIMEX base behavior, in that both base circuits use a simple passive division and are sensitive to the anode current. The tube gain varied as function of anode current (or equivalently count rate), which could introduce a rate-dependent gain modulation. This effect is related to the current drain from the last dynodes of the division chain. This effect was compensated by equipping the base with two transistors connected to the last dynodes, and stabilizing the voltage on dynodes 9 and 10. The divider drain current and division ratio remained unchanged. Fig 20 shows the modified High Voltage division chain, termed the "V1" base.

The count rate capability of the modified base circuit was tested with a double LED setup. One of these LEDs was powered from pulse generator, whereas the second LED was connected to a regulated DC current source. The LED light pulse shape was tuned to $\sim$18 ns FWHM, mimicking a scintillator pulse shape and similar to the pulse shape of the original PrimEx base (see Fig. 21).

The high-voltage bias was -1.1 kV for the new active base, where it was -1.56 kV for the original PrimEx base, to maintain about 300 mV output pulse amplitude for both PMT bases. The passive base output current is not different from the anode current, while the active base efficient output current is about 10 times higher. Fig. 6 presents the summary of our tests. The results obtained from testing of our first version "V0" base (without transistors in the division chain) are included. Note that we find the gain function as function of anode current for the PrimEx bases to be consistent with either technique: using a scintillator with gamma source and measuring the photo peak, or using the LEDs either by pulsing of DC power source.

The active base design can be seen to have improved gain stability with an efficient output signal range up to $\sim$ 160 μA. In this range, the PMT base system gain, or pulse amplitude and pulse width, remain stable to within 1%. The measured pulse rate at this current corresponds to a rate of about 1.2 MHz of 300 mV output

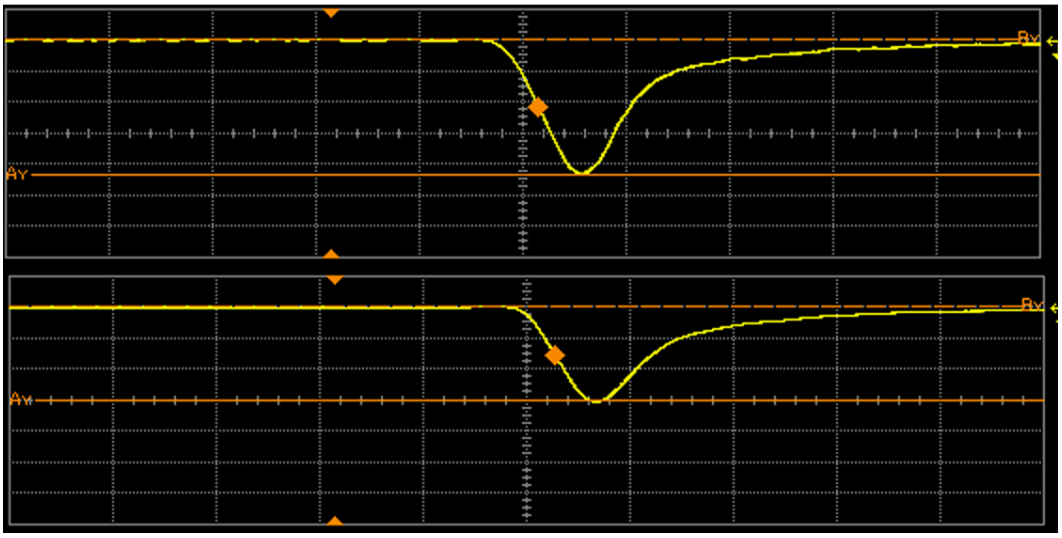

FIG. 21: *LED pulse waveforms recorded from the original PrimEx (top image) and the redesigned active base (bottom image). The horizontal scale is 20 ns per division, the vertical scale is 100 mV per division, for both images. Both records are acquired at 10 kHz LED pulse frequency.*

TABLE VII: *Comparison of the original PrimEx base (and accompanying PMT) with the modified "V1" active-base design.*

Parameter	PrimEx Base	"V1" active base
Maximum anode current	$\sim$6μA, gain variation $\pm$5%	$\sim$16μA, gain variation $\pm$1%
Maximum output pulse	unknown	-4 V, (-80 mA/50 Ohm)
Divider current	170 μA at 1.5 kV	450 μA at 1.1 kV
Maximum linear count rate	30 kHz $\pm$5%	1.2 MHz $\pm$1%

pulses. The PrimEx base during the test with the same LED light pulses on the other hand has a noticable strong PMT-and-base system gain dependence as function of count rate (or anode current). With the same LED light setting, the original PrimEx PMT/base is running out of a $\pm$5% gain stability range at a count rate of $\sim$ 30 kHz. The maximum anode current for linear operation of the active base has not changed, being proportional to the divider drain current which remains the same. Table VII summarizes the comparison between the various PMT bases.

In summary, the total count rate advantage of the newly designed active base remains unchanged between the "V0" and "V1" versions: a factor of $\sim$ 25 as compared to the PrimEx base. However, as compared to both original PrimEx base and earlier passive-divider "V0" base, the "V1" active-base design indicates a noticeable improvement of the gain stability of the complete PMT plus base system versus count rate. We plan to build, test and use such active bases for all $PbWO_4$ crystals.

[1] C.E. Carlson and J. Milana, Phys. Rev. Lett **65**, 1717-1720 (1990).
[2] E. Leader, private communications (2012).
[3] P. Monaghan, A. Accardi, M.E. Christy, C.E. Keppel, W. Melnitchouk, and L. Zhu, to be submitted (2012).
[4] A. Accardi et al., Phys. Rev. D **84**, 014008 (2011).
[5] J.C. Collins, L. Frankfurt and M. Strikman, Phys. Rev. **D56**, 2982 (1997).
[6] Report of the Jefferson Lab Program Advisory Committee (PAC38), Aug. 2011. Available online: http://www.jlab.org/exp_prog/PACpage/PAC38/PAC38_Report.pdf
[7] Report of the Jefferson Lab Program Advisory Committee (PAC32), Aug. 2007. Available online: http://www.jlab.org/exp_prog/PACpage/PAC32/PAC32_report.pdf
[8] S. V. Goloskokov and P. Kroll, Eur. Phys. J. A **47**, 112 (2011) [arXiv:1106.4897 [hep-ph]].
[9] G. R. Goldstein, J. O. Gonzales, S. Liuti, Phys. Rev. **D84** 034007 (2011).
[10] F.E. Close and W. Melnitchouk, Phys. Rev. C **79** (2009) 055202.
[11] A. Accardi, T. Hobbs, and W. Melnitchouk, JHEP 0911 (2009) 084.
[12] S.R. Brodsky, G.R. Farrar, Phys.Rev.Lett. **31** (1973) 1153.
[13] T. Horn et. al., Scaling study of the pion electroproduction cross sections and the pion form factor, Phys. Rev. C **78**, 058201 (2008); arXiv:0707.1794.
[14] A. Airapetian *et al.* [HERMES Collaboration], Phys. Lett. B **682**, 345 (2010) [arXiv:0907.2596 [hep-ex]].
[15] S. V. Goloskokov and P. Kroll, Eur. Phys. J. C **65**, 137 (2010) [arXiv:0906.0460 [hep-ph]].
[16] V. Kubarovsky *et al*, Proceedings of the 4th Workshop " Exclusive reactions at High Momentum Transfer", Newport News, VA USA, 18-21 May 2010
[17] P. Hoodbhoy and X. Ji, Phys. Rev. D**58**, 054006 (1998) [hep-ph/9801369].
[18] M. Diehl, Eur. Phys. J. C**19**, 485 (2001) [hep-ph/0101335].
[19] M.M. Kaskulov, K. Gallmeister, U. Mosel, Phys. Rev. D **78**, 114022 (2008).
[20] V. Tvaskis, M. E. Christy *et al.*, Phys. Rev.Lett. **98**, 142301 (2007); nucl-ex/0611023; E99-118 experiment, spokespersons: A. Bruell, J. Dunne, and C.E. Keppel.
[21] M. Blumenstengel *et al.*, Nucl. Phys. B **517** (2001) 37.
[22] OPAL Collaboration. R. Akers *et al.*, Z. Phys. C **68** (1995) 203.
[23] DELPHI Collaboration. P. Abreu *et al.*, Eur. Phys. J. C **6** (1999) 19.
[24] T. Sjöstrand. Comput. Phys. Commun. **39** (1986) 347; T. Sjöstrand, M. Bengtsson, Comput. Phys. Commun. **43** (1987) 367.
[25] S. Bethke, J. Phys. G **26** (2000) R27, hep-ex/0004021.
[26] C. J. Bebek *et al.*, Phys. Rev. Lett. **34** (1975) 759.
[27] C. J. Bebek *et al.*, Phys. Rev. Lett. **37** (1976) 1525.
[28] C. J. Bebek *et al.*, Phys. Rev. **D 15** (1977) 3085.
[29] T. Navasardyan *et al.*, Phys. Rev.Lett. **98**, 022001 (2007); hep-ex/0611023; E00-108 experiment, spokespersons: R. Ent, H. Mkrtchyan, and G. Niculescu.
[30] H.L. Lai *et al.*, Eur. Phys. J. **C12** (2000) 375.
[31] J. Binnewies, B. A. Kniehl, and G. Kramer, Phys. Rev. D **52** (1995) 4947.
[32] P. Bosted, R. Ent, and H. Mkrtchyan, Measurement of the Ratio $R{=}\sigma_L/\sigma_T$ in Semi-Inclusive Deep-Inelastic Scattering, proposal to Jefferson Lab PAC30.
[33] P. Bosted, R. Ent, and H. Mkrtchyan, Transverse Momentum Dependence of Semi-Inclusive Pion Production, proposal to Jefferson Lab PAC34.
[34] Hall B e1-6 run group, experiments: E99-105 (M. Guidal, et al.), E99-107 (R. Minehart, M. Taiuti, et al.), E99-108 (M. Ripani, et al.), E00-112 (K. Joo, G. Niculescu, B. Raue, et al.)
[35] Hall B e1-dvcs run group, coordinator: S. Stepanyan, experiments: E06-003 (V. Burkert, L. Elouadrhiri, M. Garcon, R. Niyazov, et al.), 01-113 (V. Burkert, L. Elouadrhiri, M. Garcon, et al.)
[36] Y. Roblin and F. Sabatie, Deeply Virtual Compton Scattering at 6 GeV, proposal to Jefferson Lab PAC18.
[37] M. Bertin, C. Hyde, C. Munoz-Camacho, and J. Roche, Separation of Deeply Virtual Photon and pi0 production observables of unpolarized protons, proposal to Jefferson Lab PAC31.

[38] K. Joo, M. Ungaro, C. Weiss, V. Kubarovsky and P. Stoler, Hard Exclusive Electroproduction of π^0 and η with CLAS12, JLab 12 GeV Proposal PR12-06-101, 2006.

[39] E. Fuchey, A. Camsonne, C. Muñoz Camacho, M. Mazouz, G. Gavalian, E. Kuchina, M. Amarian and K. A. Aniol, M. Beaumel, H. Benaoum, P. Bertin, M. Brossard, M. Canan, J.-P. Chen, E. Chudakov, B. Craver, F. Cusanno, C. W. de Jager, A. Deur, C. Ferdi, R. Feuerbach, J.-M. Fieschi, S. Frullani, M. Garçon, F. Garibaldi, O. Gayou, R. Gilman, J. Gomez, P. Gueye, P. A. M. Guichon, B. Guillon, O. Hansen, D. Hayes, D. W. Higinbotham, T. Holmstrom, C.E. Hyde, H. Ibrahim, R. Igarashi, F. Itard, X. Jiang, H. S. Jo, L. J. Kaufman, A. Kelleher, A. Kolarkar, G. Kumbartzki, G. Laveissiere, J. J. LeRose, R. Lindgren, N. Liyanage, H.-J. Lu, D. J. Margaziotis, Z.-E. Meziani, K. McCormick, R. Michaels, B. Michel, B. Moffit, P. Monaghan, S. Nanda, V. Nelyubin, M. Potokar, Y. Qiang, R. D. Ransome, J.-S. Réal, B. Reitz, Y. Roblin, J. Roche, F. Sabatié, A. Saha, S. Sirca, K. Slifer, P. Solvignon, R. Subedi, V. Sulkosky, P. E. Ulmer, E. Voutier, K. Wang, L. B. Weinstein, B. Wojtsekhowski, X. Zheng, and L. Zhu (Jefferson Lab Hall A Collaboration), Phys. Rev. C **83**, 025201 (2011) [arXiv:1003.2938 [nucl-ex]].

[40] JLab experiment E12-06-114 A. Camsonne, C. Hyde, C. Muñoz Camacho, J. Roche, *et al.*, *"Measurements of the electron-helicity dependent cross-sections of deeply virtual Compton scattering in Hall A at 11 GeV"* . Approved for 100 days. arXiv:nucl-ex/0609015, and `http://wwwold.jlab.org/exp_prog/proposals/11prop.html`

[41] C. Muñoz Camacho, A. Camsonne, M. Mazouz, C. Ferdi, G. Gavalian, E. Kuchina, M. Amarian, K. A. Aniol, M. Beaumel, H. Benaoum, P. Bertin, M. Brossard, J.-P. Chen, E. Chudakov, B. Craver, F. Cusanno, C. W. de Jager, A. Deur, R. Feuerbach, J.-M. Fieschi, S. Frullani, M. Garçon, F. Garibaldi, O. Gayou, R. Gilman, J. Gomez, P. Gueye, P. A. M. Guichon, B. Guillon, O. Hansen, D. Hayes, D. Higinbotham, T. Holmstrom, C. E. Hyde-Wright, H. Ibrahim, R. Igarashi, X. Jiang, H. S. Jo, L. J. Kaufman, A. Kelleher, A. Kolarkar, G. Kumbartzki, G. Laveissière, J. J. LeRose, R. Lindgren, N. Liyanage, H.-J. Lu, D. J. Margaziotis, Z.-E. Meziani, K. McCormick, R. Michaels, B. Michel, B. Moffit, P. Monaghan, S. Nanda, V. Nelyubin, M. Potokar, Y. Qiang, R. D. Ransome, J.-S. Réal, B. Reitz, Y. Roblin, J. Roche, F. Sabatié, A. Saha, S. Sirca, K. Slifer, P. Solvignon, R. Subedi, V. Sulkosky, P. E. Ulmer, E. Voutier, K. Wang, L. B. Weinstein, B. Wojtsekhowski, X. Zheng, and L. Zhu [Jefferson Lab Hall A Collaboration], Phys. Rev. Lett. **97**, 262002 (2006) [nucl-ex/0607029].

[42] M. Mazouz, A. Camsonne, C. Muñoz Camacho, C. Ferdi, G. Gavalian, E. Kuchina, M. Amarian, K. A. Aniol, M. Beaumel, H. Benaoum, P. Bertin, M. Brossard, J.-P. Chen, E. Chudakov, B. Craver, F. Cusanno, C. W. de Jager, A. Deur, R. Feuerbach, J.-M. Fieschi, S. Frullani, M. Garçon, F. Garibaldi, O. Gayou, R. Gilman, J. Gomez, P. Gueye, P. A. M. Guichon, B. Guillon, O. Hansen, D. Hayes, D. Higinbotham, T. Holmstrom, C. E. Hyde, H. Ibrahim, R. Igarashi, X. Jiang, H. S. Jo, L. J. Kaufman, A. Kelleher, A. Kolarkar, G. Kumbartzki, G. Laveissière, J. J. LeRose, R. Lindgren, N. Liyanage, H.-J. Lu, D. J. Margaziotis, Z.-E. Meziani, K. McCormick, R. Michaels, B. Michel, B. Moffit, P. Monaghan, S. Nanda, V. Nelyubin, M. Potokar, Y. Qiang, R. D. Ransome, J.-S. Réal, B. Reitz, Y. Roblin, J. Roche, F. Sabatié, A. Saha, S. Sirca, K. Slifer, P. Solvignon, R. Subedi, V. Sulkosky, P. E. Ulmer, E. Voutier, K. Wang, L. B. Weinstein, B. Wojtsekhowski, X. Zheng, and L. Zhu [Jefferson Lab Hall A Collaboration], Phys. Rev. Lett. **99**, 242501 (2007) [arXiv:0709.0450 [nucl-ex]].

[43] JLab Hall A DVCS experiment E07-007 A. Camsonne, C. Hyde, C. Muñoz Camacho, J. Roche, *et al.*, *"Complete separation of Deeply Virtual Photon and π^0 electro-production observables of unpolarized protons"*, `http://hallaweb.jlab.org/experiment/DVCS/`

[44] J.J. Kelly et al., Phys. Rev. Lett. **95**, 102001 (2005); nucl-ex/0509004.

[45] J.J. Kelly, The $p(e,e'N)pi$ Reaction with Harp, TJNAF proposal 93-013, 1993.

[46] G. Laveissiere et al., Phys. Rev. **C69**, 045203 (2004).

[47] T. Pospischil et al., Eur. Phys. J. **A12**, 125 (2001).

[48] C.N. Brown et al., Phys. Rev. Lett. **27**, 1611 (1971).

[49] Y. Liang *et al.*, nuc-ex/0410027; E94-110 experiment, spokesperson: C.E. Keppel.

[50] I. Bedlinskiy, V. Kubarovsky, S. Kuleshov, O. Pogorelko, CLAS NOTE 2004-040 (2004).

[51] L. Nagornaya et al., IEEE Transactions on Nuclear Science, Vol. 44, No. 3, p.866, June 1997.

[52] R. Y. Zhu et al., IEEE Transactions on Nuclear Science, Vol. 45, No. 3, p.686, June 1998.

[53] M.Guidal, J.-M. Laget, M. Vanderhaeghen, Nucl. Phys. **A 627** (1997) 645.

[54] M. Guidal, J.M. Laget, and M. Vanderhaeghen, Phys. Rev. **C61** 025204 (2000).

[55] M. Vanderhaeghen, P.A.M Guichon, and M. Guidal, Phys. Rev. Lett. **80**, 5064 (1998).

[56] S. V. Goloskokov and P. Kroll, private communication (2012).

[57] P. Geiger, Ph.D. Dissertation, Heidelberg University (1998), unpublished.
[58] H. Mkrtchyan *et al.*, Phys. Lett. B **65** (2008) 20.
[59] I.T. Obukhovsky, private communication (2007); arXiv:0706.1844v1 (2007).
[60] J.M Laget, Phys. Lett. **B 695**, 199 (2011).
[61] M. Kaskulov et al., arXiv:1103.2097 (2011).
[62] M. Kubantsev et al., Performance of the Primex Electromagnetic Calorimeter, arXiv:physics/0609201, 22 Sep. 2006; A. Gasparyan, Performance of PWO crystal Detector for a High Resolution Hybrit Electromagnetic Calorimeter at Jefferson Lab., Proceed. X Int. Conf. Calorimetry in Particle Physics, Perugia, Italy, 29 March-2 April 2004, pp. 109-115.
[63] G. Franzoni et.al, Nucl. Instrum. Meth. A628, 90 (2011).
[64] V. A. Batarin et.al, (BTeV electromagnetic calorimeter group), Nucl. Instrum. Meth. A512, 488 (2003), hep-ex/0210011.
[65] Pavel Degtiarenko, private communication.
[66] Bitao Hu, The analysis of primex test run on September 15. PRIMEX analysis documentation.